Learning Induced Modification of Neural Responses and Neuron-Neuron Interactions in the Primary Somatosensory Cortex

by

Yexin Yang

A dissertation submitted in partial fulfillment
of the requirements for the degree of
Doctor of Philosophy
(Molecular, Cellular, and Developmental Biology)
in the University of Michigan
2023

Doctoral Committee:

Assistant Professor Sung Eun 'Samuel' Kwon, Chair
Associate Professor Sara Aton
Professor Victoria Booth
Professor Richard Hume

Yexin Yang

kathyang@umich.edu

ORCID iD: 0000-0002-6849-3601

Dedication

This thesis is dedicated to my family and friends.

For their unconditional love and support through my academic journey.

Acknowledgements

I would like to begin by expressing my deepest gratitude to my advisor, Dr. Samuel Kwon, for providing invaluable guidance in both science and career development. Your constant support and encouragement during times when I lacked confidence were instrumental in my success. I am also grateful for your patience in my trial and error and for the constructive criticism that has helped me grow as a scientist.

I also want to acknowledge the help and advice from my dissertation committee members, Dr. Sara Aton, Dr. Victoria Booth, Dr. Richard Hume, and Dr. Monica Dus. Your contributions have been indispensable to my research, and I am honored to have had the privilege of working with such distinguished scholars.

I would like to express my heartfelt appreciation to Mary Carr, our graduate coordinator, for her tireless dedication to ensuring the success of all graduate students in our program, and for her genuine concern for my well-being during challenging times. I also thank the MCDB department for their financial support during difficult times.

I am grateful to my lab members at the Kwon Lab for providing me with a scientific home for the past five years. Meiling Zhao, Max Oginsky, Chia-Wei Chang, Hao 'Johnny' Shen, and Samantha Grudzien, thank you for sharing your insights and expertise with me, and for your help with experiments and analyses.

Finally, I would like to thank everyone in the laboratory neighborhood for fostering a collaborative and supportive research environment. Your contributions have been essential to the success of our scientific endeavors.

Table of Contents

List of Tables

List of Figures

List of Acronyms

whisker primary somatosensory cortex	wS1
Layer 2/3; Layer 1; Layer 4; Layer 5	L2/3; L1; L4; L5
central nerve system	CNS
trigeminal ganglia	TG
dorsal root ganglia	DRG
principal trigeminal nucleus	Pr5
ventral posteromedial nucleus	VPM
posteromedial complex	POm
interneurons	INs
secondary sensory cortex	wS2
primary motor cortex	M1
secondary motor cortex	M2
Primary Auditory Cortex	A1
orbitofrontal cortex	OFC
Posterior parietal cortex	PPC
Perirhinal Cortex	PRh
primary visual cortex	V1
Somatostatin-expressing	SST
Parvalbumin-expressing	PV

vasoactive intestinal peptide-expressing	VIP
anterior lateral motor cortex	ALM
Pyramidal neuron	PYR
Hit Rate	HR
False Alarm Rate	FAR
Fraction Correct	FC
receiver operating characteristic	ROC
Interquartile range	IQR
out-of-task	OOT
Stimulus Probability	SP
area under the ROC curve	AUC
Confidence interval	CI

Abstract

Perceptual learning alters the representation of sensory input in primary sensory cortex. Alterations in neuronal tuning, correlation structure and population activity across many subcortical and cortical areas have been observed in previous studies. However, relationships between these different neural correlates - and to what extent they are relevant to specific perceptual tasks - are still unclear. In this study, we recorded activity of the layer 2/3 (L2/3) neuronal populations in the whisker primary somatosensory cortex (wS1) using *in vivo* two-photon calcium imaging as mice were trained to perform a self-initiated, whisker vibration frequency discrimination task. Individual wS1 neurons displayed learning-induced broadening of frequency sensitivity within task-related categories only during task performance, reflecting both learning and context-dependent enhancement of category selectivity. Learning increased both signal and noise correlations within pairs of neurons that prefer the same stimulus category ('within-pool'), whereas learning decreased neuronal correlations between neuron pairs that prefer different categories ('across-pool'). Increased noise correlations in trained animals resulted in less accurate decoding of stimulus categories from population activity but did not affect decoding of the animal's decision to respond to stimuli. Importantly, within-pool noise correlations were elevated on trials in which animals generated the learned behavioral response. We demonstrate that learning drives formation of task-relevant 'like-to-like' L2/3 subnetworks in the primary sensory cortex that may facilitate execution of learned behavioral responses.

Chapter 1 Introduction

1.1 Sensory System

Our nervous system processes external sensory inputs and converts them into percepts, which are then used to guide decision-making and motor behaviors. Sensory processing involves steps of encoding of sensory stimuli, transmission to motor areas, decision-making, action planning, and execution. Understanding how these steps are mediated at the level of a neural circuit is one of the biggest challenges in neuroscience. Mechanisms by which peripheral neurons convert external sensory stimuli into electrical signals have been determined in sufficient detail (Abraira and Ginty, 2013; Koerber and Woodbury, 2002). Studies show that peripheral processing of external sensory input is reliable such that the same stimulus presented with repetition evokes invariant responses in individual peripheral sensory neurons, and collectively the population encodes a great amount number of features of external stimuli (Zucker and Welker, 1969). On the other hand, neurons in the sensory cortex show substantial variability in their responses even during repeated presentations of an identical stimulus, and therefore they do not reliably encode sensory information (Tolhurst et al., 1983). In the sensory cortex, sensory information is reliably represented by the population of neurons, rather than individual neurons (Schreiner et al., 1978; Werner and Mountcastle, 1963). Cortical representation of sensory information is also context-dependent and shows significant learning-induced plasticity, which is clearly distinct from the invariant sensory representations at the periphery. Substantial evidence

indicates that improvements in sensory-based task performance correlate with an improved representation of relevant stimulus features by individual cortical neurons (Cossell et al., 2015; Schoups et al., 2001; Xin et al., 2019). On the other hand, learning-induced modifications in the 'population' activity remain poorly understood. Most prior studies focus on changes in tuning curves of individual cortical neurons, which are treated as independent units of computation. Critically, however, stimulus-evoked activities of individual cortical neurons are not only unreliable but also correlated with each other (Petersen et al., 2003; Smith and Kohn, 2008; Zohary et al., 1994). The amount of correlated neural activity is thought to be a limiting factor for the population-level representation of sensory stimuli (Gawne and Richmond, 1993; Kafashan et al., 2021). The role of neuronal correlations in encoding of sensory information is a topic of active investigation in the field (Panzeri et al., 2022). Questions of whether and how perceptual learning alters tuning curves of individual neurons and neuron-neuron correlations are of fundamental importance for understanding the neural mechanisms of learning. My thesis focuses on how neuronal representation of sensory input changes during perceptual learning. Specifically, I aim to characterize learning-induced changes in response properties of individual cortical neurons and to determine their relationships with neuronal correlations. In doing so, I aim to provide new insights into neural mechanisms of perceptual learning.

I use the whisker wS1 as a model system for several reasons. First of all, whisker sensation is one of the primary sources of information that mice use to interact with surrounding environments, which permits sophisticated behavioral tasks to be designed for testing specific hypotheses about neuron-behavior relationships. Second, the

whisker system, which extends from the whiskers to the wS1, is readily accessible for neural recording and experimental manipulations in head-restrained mice. Also, there is a substantial body of work regarding basic properties of neuronal responses in the wS1. For these reasons, the wS1 is widely used for studying relationships between neuronal population activity and learning. Here I provide a brief overview of the anatomical connectivity and basic functions of the whisker signaling pathway. Then I review the current understanding of population codes in the sensory cortex.

1.1.1 Whisker Signaling Pathway

The somatosensory system is essential for our ability to sense body movement, touch, temperature, pain, and so on. The whisker-mediated touch system has been widely used in studies of tactile perception (Van der Loos and Woolsey, 1973; Woolsey and Van der Loos, 1970). Touch sensation begins at the peripheral sensors of tactile input – whisker follicles and the skin. Attached to these sensors are specialized epidermal cells such as Merkel cells that act as mechanoreceptors (Hoffman et al., 2018; Merkel, 1875; Woo et al., 2014). Mechanoreceptors transduce physical movement into electrical signals, which then propagate to trigeminal ganglia (TG) or dorsal root ganglia (DRG) through sensory afferent nerves (Coste et al., 2010; Melzack and Wall, 1962; Zucker and Welker, 1969). Sensory neurons innervating facial areas (including whiskers) have their cell body located in the TG, whereas others have their cell bodies located in the DRG. Sensory afferents are categorized by the diameter of nerves and conduction velocity. Aβ afferent nerves have a conduction speed in the range of 30-70m/s and normally innervate hair follicles, Merkel cells, and some muscles (Haeberle and Lumpkin, 2008; Li and Bak, 1976). The molecular mechanism of

mechanotransduction was not revealed until 2010 when the Nobel prize laureate Ardem Patapoutian identified Piezo2 as the gene encoding mechanoreceptor (Coste et al., 2010). Piezo2 is expressed in Merkel cells and Aβ fibers (Woo et al., 2014). This gene encodes the mechanosensitive cation channel PIEZO2 that opens rapidly in response to the change of mechanical force in the cell membrane. The opening of PIEZO2 depolarizes the membrane potential and leads to the generation of action potentials in Aβ fibers, which then transmit the touch signal to the central nerve system (CNS).

Spiking activities encoding tactile input travel through TG and reach the principal trigeminal nucleus (Pr5) in the brainstem (Erzurumlu and Killackey, 1979; Lo et al., 1999; Veinante and Deschênes, 1999). Pr5 neurons form glutamatergic synapses with the ventral posteromedial nucleus (VPM) in the thalamus (Erzurumlu et al., 1980; Smith, 1975). VPM neurons send glutamatergic projections to wS1 (Jensen and Killackey, 1987; Killackey, 1973; Woolsey and Van der Loos, 1970). Neurons responsive to the same whisker sensation are topographically arranged, forming ‘barrelettes’ in the brainstem, ‘barreloids’ in the thalamus, and ‘barrel’ columns in the wS1 (Woolsey and Van der Loos, 1970). For this reason, the primary whisker somatosensory cortex is also called the “barrel” cortex.

Along this ascending pathway of whisker signaling, information is mainly transmitted via feedforward excitatory glutamatergic synapses. At the periphery, features of whisker deflection are represented by the firing rate (i.e. action potential frequency) in TG. As the stimuli travel up the ascending pathway, the neuronal representation of tactile stimuli evolves. The thalamus is an important station gating the entrance of neuronal signals to the cortex. In the VPM areas of the thalamus, neurons

relay whisker-evoked neural activities to layer 4 (L4) of wS1 through glutamatergic projections (Figure 1A). Reciprocal connections are found between higher-order thalamic areas such as the posteromedial complex (POm) and layer 1 and 5a of wS1 (Figure 1A). Recent *in vivo* recording studies have shown that POm neurons encode complex sensory features that involve multiple whiskers sensation, and this area is proposed to be a hub of plasticity during sensory-guided learning. However, the full

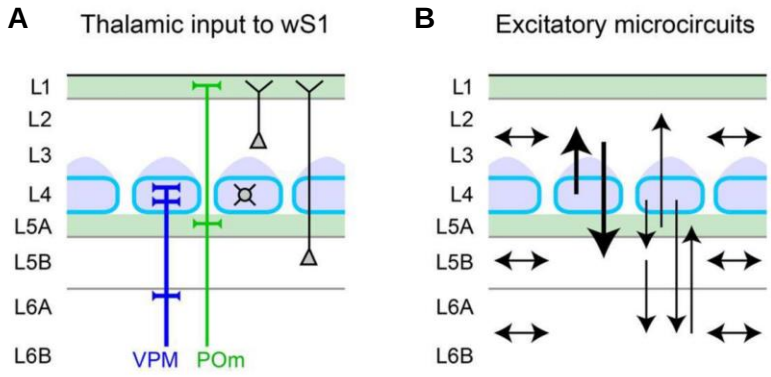

Figure 1. Schematic of thalamic inputs to wS1 and intra-cortical excitatory microcircuits. (Petersen, 2019)

functions of thalamic-cortical feedback loops are still unclear.

1.1.2 Laminar Organization & Function of wS1

As briefly mentioned in the section above, wS1 is organized into different layers, through which sensory representing activity is further processed for learning and motor transmission. This section will lay out the basic connectivity and functions of these cortical layers.

As shown in Figure 1, neurons in wS1 develop into six layers with distinct compositions of cell types and input/output projections. Based on the anatomical specificity of cortical layers, each layer is thought to have a unique function in cortical computations. The excitatory neurons in L4 receive direct projection from VPM neurons

and send feedforward glutamatergic projections into both excitatory pyramidal neurons and inhibitory interneurons (INs) in L2/3 (L2/3) (Figure 1B). L2/3 pyramidal neurons innervate layer 5 (L5) neurons that send output projections to subcortical areas including basal ganglia and the spinal cord (Figure 1B). L2/3 neurons also send long-range projections to distal cortical areas including the secondary somatosensory cortex (wS2), primary motor cortex (M1) and higher-order associative regions (e.g. orbitofrontal cortex/OFC, Posterior parietal cortex/PPC), thus participating in multiple cortico-cortical pathways. The six-layer cytoarchitecture is conserved across different species and different sensory modalities. The exact function of different cortical layers is under active investigation.

As Table 1 summarizes, the primary sensory cortices receive and integrate multiple cortical inputs that carry diverse information including sensory reafferent (movement related) input, motor feedback, and reward-contingency from high-order cortical regions (Petersen, 2019). For example, M2 neurons projecting to the primary auditory cortex (A1) transmit signals encoding reafferent sound that is generated during self-initiated movement (Schneider et al., 2018). This projection targets local parvalbumin (PV) neurons in A1 that suppress the reafferent-evoked response (Schneider et al., 2018). OFC neurons project to the primary visual cortex (V1) to recruit local INs to reduce the response amplitude when presented with reward-irrelevant stimuli, thus facilitating sensory-based associative learning (Liu et al., 2020). Studies on cortical connectivity also found reciprocal projections between wS1 and PPC (Wang et al., 2012). Specifically, the PPC projecting wS1 neurons serve as an intermediate step of the POm-wS1-PPC pathway that perhaps contribute to whisking-informed spatial

reconstruction (Lee et al., 2011). While recent studies uncovered the layer-specific sensorimotor integration process at PPC (Mohan et al., 2019), it is still unclear what activity the feedback projection from PPC to wS1 carries. A major goal of cortical computation involves extraction and amplification of sensory information that is most relevant to ongoing behavioral demands (Peron et al., 2020). The task-relevant sensory information is then used to drive motor responses.

Table 1. A summary of top-down cortical inputs to wS1 and their functions from previous studies.

Cortical Projections	**Type of Activity**	**Citation**
M1 → wS1	Motor related signals	(Kinnischtzke et al., 2016; Kinnischtzke et al., 2014; Lee et al., 2013)
M2 → wS1, A1	Self-generated movement signals - contribute to the sensory stimulus-evoked late activity in wS1	(Manita et al., 2015; Schneider et al., 2018)
wS2 → wS1	Perceptual results; Modulates activity and tuning in wS1	(Kwon et al., 2016; Minamisawa et al., 2018)
OFC → wS1, V1	Value prediction error; reward-irrelevant stimuli	(Banerjee et al., 2020; Liu et al., 2020)
PPC → wS1	Within the POm-wS1-PPC pathway that contribute to whisking-informed spatial reconstruction	(Wang et al., 2012)
Perirhinal Cortex (PRh) → wS1	Facilitate fast firing in wS1 during hit trials; promote learning	(Doron et al., 2020)

L2/3 neurons in the sensory cortex have been widely used in studies focusing on cortical plasticity, because L4→L2/3 intra-columnar synapse is highly plastic (Allen et al., 2003; Clancy et al., 2014; Feldman, 2000; Feldman and Brecht, 2005; House et al., 2011). Importantly, cortical activities in L2/3 are sufficient to bias behavioral decisions, suggesting that they may play a key role in generating task-relevant perceptions. Studies using optogenetic activation on layer-specific ensembles of pyramidal neurons successfully cause perception in animals and drive associated behaviors (Dalgleish et al., 2020; Houweling and Brecht, 2008; Marshel et al., 2019; Tanke et al., 2018). Thus, L2/3 is a suitable target for studies that focus on learning-dependent changes in sensory representation.

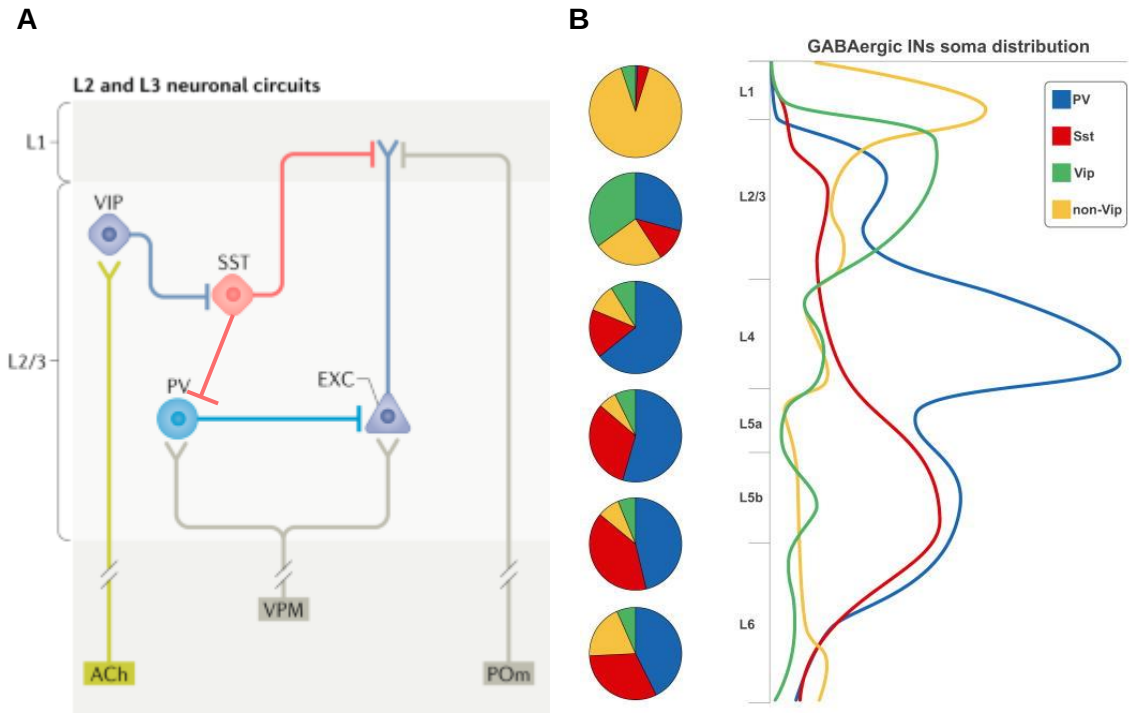

Figure 2. Schematic of inhibitory INs microcircuits and distribution across six layers of wS1. (A) Microcircuits by major inhibitory interneurons and excitatory pyramidal neurons (EXC) in L2/3 of wS1. Modified to add inhibition from SST to PV. (Petersen, 2019); (B) GABAergic INs cell body distribution across six layers of wS1(Tremblay et al., 2015).

In addition to its complex connectivity, the diverse cell type composition in wS1 also plays an important role in sensory processing, including glutamatergic excitatory neurons and GABAergic inhibitory neurons (Figure 2). There are three major types of GABAergic INs which whose activity are known to contribute to sensory-based learning. First, vasoactive intestinal peptide (VIP, ~15% of INs in all layers)-expressing neurons receive synchronized cholinergic inputs from the basal forebrain during reinforcement learning, disinhibiting downstream excitatory principle neurons and increasing the gain of cortical response to the task-related sensory stimuli (Pi et al., 2013). Second, Somatostatin (SST, ~30% IN in all layers)-expressing INs receive GABAergic input from VIP INs and project to the distal dendrites of L2/3 pyramidal neurons at layer 1 (L1). As a result, cholinergic inputs to VIP disinhibit pyramidal neurons through the suppression

of SST neurons (Pfeffer et al., 2013; Pi et al., 2013). Third, Parvalbumin (PV, ~40% IN in all layers)-expressing neurons are fast-spiking cells and receive direct inputs from VPM. In L2/3, L4, and L5, PV INs are electrically connected through gap junctions (Fukuda, 2017; Hatch et al., 2017; Hestrin and Galarreta, 2005). Importantly, the coupled PV INs in L2/3 provide local inhibitory feedback to nearby pyramidal neurons (Fukuda et al., 2006), contributing to the appropriate timing of the activity of principal cells to reliably represent sensory stimuli during cortical sensory processing. Studies have also shown that PV activity anti-correlates with correct performance, gating the goal-directed sensorimotor transformation through modulating the activity of adjacent excitatory neurons (Sachidhanandam et al., 2016). Taken together, PV neurons are thought to contribute to the sparse activity of L2/3 excitatory pyramidal neurons during stimulus presentation (see below). Reward-associated stimuli, when they are coupled with neuromodulators like acetylcholine, cause excitation of a subset of pyramidal neurons through the disinhibitory motif that consists of VIP and SST INs.

1.1.3 Sparse Activity

In vivo whole cell recording of L2/3 neurons in wS1 suggested that the rapid recruitment of GABAergic INs hyperpolarizes excitatory neurons and suppresses their spontaneous activity and stimulus-evoked spiking activities (Crochet et al., 2011). Indeed, only about 10% of the excitatory cortical neurons in L2/3 of wS1 generate action potentials in response to whisker stimuli, exhibiting lower responsiveness compared to peripheral and subcortical neurons (Petersen, 2019), consistent with sparse population activity. As aforementioned, PV INs are shown to be involved in the appropriate timing of activities of principal cells, which could be a cause of the low responsiveness of

pyramidal neurons. Specifically, experiments have shown optogenetic inactivation of PV INs leads to an increase in the responsiveness of pyramidal neurons to whisker stimulation in anesthetized rats (Yeganeh et al., 2022). In addition, the NMDARs at feedback synapses on PV INs mediate nonlinear integration of excitatory inputs, contributing to the recruitment and stabilization of functional assemblies of principle neurons to represent sensory signals among cortical noise (Cornford et al., 2019). Patients with autism spectrum disorder experience abnormal sensory processing and learning. The deletion of *Shank3* in wS1 inhibitory neurons, as a common mouse model for autism spectrum disorder, causes hyperactivity in L2/3 and learning deficit, suggesting that fine-tuned activity is one feature of normal learning (Chen et al., 2020).

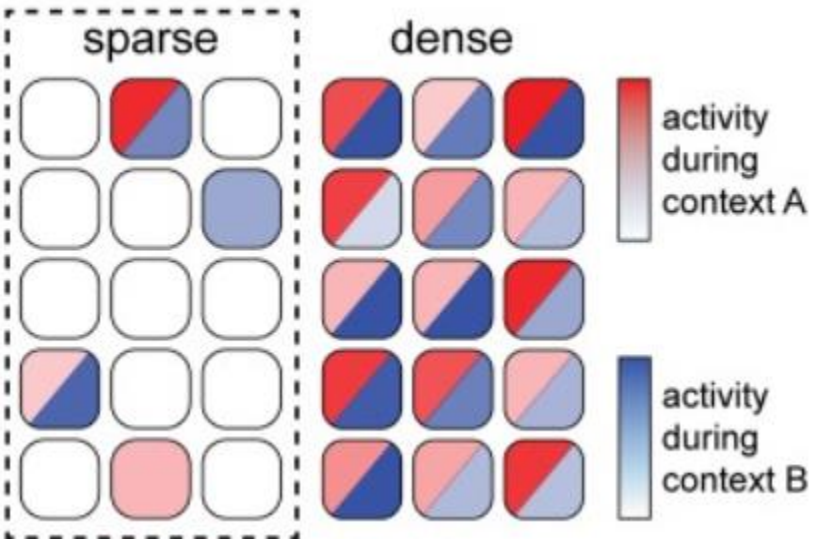

Figure 3. Illustration of sparse code and dense code of two stimulation contexts. Each square represents a neuron. The color saturation indicates the activity strength evoked by the according stimulation context. Sparse code utilizes a small ensemble of neurons to encode a particular stimulus. Dense code uses the weighted sum of all neurons to encode a particular stimulus. (Beyeler et al., 2019)

Sparse activity (Figure 3), is a common strategy employed by various sensory systems (Barth and Poulet, 2012). It is considered superior to dense coding in a neuron population because it suffers less from neuron-neuron cross-talk but also maintains large encoding capacity given a fixed number of neurons in a population (Beyeler et al.,

2019; Marshel et al., 2019). Experiments using microstimulation of wS1 showed that sparse activation is sufficient for driving perceptions and actions with lower and upper bounds of ~14-37 pyramidal neurons in wS1 (Dalgleish et al., 2020; Houweling and Brecht, 2008). Sparse activity presents metabolic efficiency and functional advantages to the cortical circuits (Panzeri et al., 2015). In particular, sparse activity allows high selectivity of sensory features with remaining coding flexibility, which balances the trade-off between the needs to differentiate similar stimuli and also to generalize various stimuli (Barak et al., 2013). Moreover, sparse activity allows the integration of top-down modulation with the bottom-up sensory input. In many sensory modalities, the sparseness of neural activity was found higher during wakefulness than during anesthesia (Ranjbar-Slamloo and Arabzadeh, 2019; Rinberg et al., 2006), which could be caused by a reduction of recurrent inhibition that comes from cortico-cortical feedback projections, suggesting that top-down inputs can temporarily regulate the firing states of L2/3 pyramidal neurons. The integration of multisensory information through sparse activity is key for reliable and robust sensorimotor learning.

The key challenge associated with sparse activity is the robust extraction of small-group activity from a relatively large population and the transmission of activity to downstream areas. In particular, adequate signal-to-noise ratio is essential for ensuring robustness, which will be further discussed in later sections within the discussion of population codes.

1.1.4 Signal Propagation and Sensorimotor Transition

Whether and how population activity of wS1 neurons guide decision-making and motor planning is a fundamental question in neuroscience. Here I review some progress

that has been made on this issue over the years. It is proposed that the sensory information in wS1 is increasingly transformed into motor activities along the pathways that connect sensory cortices to motor-related areas (de Lafuente and Romo, 2005, 2006; Esmaeili et al., 2020; Kwon et al., 2016). The monosynaptic projections from wS1 to wS2 and M1 play important roles in detecting whisker stimulation and generating conditioned behavioral responses (Esmaeili et al., 2022; Esmaeili et al., 2020; Kwon et al., 2016). Interestingly, there is minimal overlap between wS2-projecting neurons and M1-projecting neurons located in L2/3 of wS1 (Chen et al., 2013; Sorensen et al., 2015; Yamashita et al., 2013), indicating that these are two parallel routes of conveying distinct activities from L2/3 neuron populations. To study the distinct sensorimotor functions emerging from these two parallel pathways, *in vivo* neuron recording, and region-specific inactivation were used in several previous studies.

Findings from these studies show that behavioral decision-related activities are present in wS2-projecting wS1 neurons in mice performing whisker-based detection tasks (Kwon et al., 2016). The reciprocal connections between wS1 and wS2 are required for performance during whisker-guided perceptual tasks. A recent study from the Peterson CH lab explained how projection from wS2 to the motor cortex changes as animals become expert at whisker detection tasks. In particular, the increase of putative excitatory inputs from wS2 to the secondary motor cortex (M2) increased the ratio of excitation to inhibition in M2, which potentially gives rise to the increase in E/I ratio in the higher order motor cortex (i.e. anterior lateral motor cortex / ALM) and contributes to sensory-evoked motor planning (Esmaeili et al., 2022). Taken together, these studies

suggest that wS1, wS2 and M2 may constitute the cortical circuit that transforms whisker sensation into appropriate behavioral responses.

Wide-field *in vivo* calcium imaging in mice performing whisker-guided behavioral tasks found sequential activities first evoked in wS1 and then in M1. M1-projecting neurons in wS1 integrate active whisker movements and passive touch sensation delivered to the whiskers. Interestingly, M1 is found to have enhanced inhibition during late sessions of whisker detection training, which is speculated to decrease spontaneous whisker movement, reduce confounding whisker sensation, and therefore facilitate task performance (Esmaeili et al., 2022). Pathway-resolved recordings showed that the wS1-M1 pathway robustly encodes passive whisker stimulation. The wS1-wS2 pathway, on the other hand, encodes complex sensory features that contribute to categorizing or discriminating stimuli (Chen et al., 2013; Yamashita et al., 2013). Furthermore, the wS1-wS2 pathway transmits decision-related activities, which develop through learning (Kwon et al., 2016; Yamashita and Petersen, 2016).

In summary, propagating behaviorally relevant signals from wS1 to downstream areas is as important as the representation of sensory stimuli within wS1. While spare activity facilitates the encoding of sensory stimuli, it may not be beneficial for the propagation of task-relevant signals to downstream areas.

1.1.5 Correlated Neural Activity in the Neocortex

We have discussed how individual neurons or microcircuits encode sensory features, but it is important to consider neuron population-level changes in the wS1 region that lead to performance improvement during learning, because sensory information is reliably encoded by neuronal populations in the sensory cortex. In a

simplistic view, the amount of sensory information encoded by neuronal populations will grow with an increasing number of neurons in the population, as trial-by-trial fluctuation of sensory responses ('noise') will be cancelled out more effectively by averaging across a greater number of neurons. However, trial-by-trial fluctuations of sensory responses are correlated – weakly but positively – across neuronal populations and cannot be averaged out. Neuronal correlation is an emergent property of the sensory cortex that arises from synaptic connections and/or shared synaptic input. Neuronal correlations in a population are proposed to shape the encoded information by individual neurons and facilitate propagation to downstream brain regions. However, a prediction based on theoretical studies is that neuronal correlation limits the amount of sensory information encoded by neuronal populations (Bartolo et al., 2020; Kafashan et al., 2021; Petersen et al., 2001; Rumyantsev et al., 2020; Zohary et al., 1994). Thus, investigating the role of neuronal correlation will help understand how the neuron population functions to represent sensory information.

Prior studies in different cortical areas have estimated pairwise neuronal correlation using the Pearson correlation coefficient of trial-by-trial fluctuations around the mean between pairs of neurons (Cohen and Kohn, 2011). Typical values are small positive numbers, ranging from 0.05 – 0.25 (Cohen and Kohn, 2011; Ecker et al., 2010; Zohary et al., 1994). Despite being relatively small in magnitude, pairwise neuronal correlations are thought to severely limit the sensory information encoded by a neuronal population, although this is debatable (see below) (Adibi et al., 2013; Bartolo et al., 2020; Chen et al., 2015; Kafashan et al., 2021; Petersen et al., 2001; Rumyantsev et al., 2020; Sanayei et al., 2018; Tremblay et al., 2015). In most previous studies, the

average of all pairwise correlations from a neuron population was used to estimate the magnitude of neuronal correlation within a population. However, the ”structure” of neuronal correlations has been often overlooked in these studies. This is important to consider because neurons with similar tuning properties and feature selectivity tend to connect with each other more often than those with dissimilar characteristics, which results in elevated neuronal correlations among similarly tuned neurons (Cossell et al., 2015; Ko et al., 2011). Plasticity processes during learning exerts varying degrees of impact on neuronal correlations depending on tuning and feature selectivity of different pairs. Therefore, to test the impact of learning, it is critical to characterize the “matrix” of neuronal correlations instead of a simple average.

It remains highly controversial whether neuronal correlation contributes to or reduces coding efficiency of a neuron population. Conventionally, encoding efficiency is studied with the assumption that downstream decoders are optimal. Under this assumption, the sparse coding theory suggests that correlated neuronal activity will decrease the encoding capacity, thus reducing the coding efficiency. However, when we ease the unrealistic assumption, the need to robustly propagate relevant information to downstream regions is taken into consideration, making correlated activity sometimes beneficial for coding efficiency. We will discuss this more in the later section.

1.1.6 Types of Correlation

To put these concepts into experimental context, pairwise correlation can be characterized as signal and noise correlations (Figure 4). Signal correlation is a measurement of tuning similarity comparing two neurons (Figure 4A,C). The tuning property of a single neuron depicts averaged stimulus-evoked responses as a function

of sensory features. The more overlap between two neuronal tuning curves, the higher signal correlation exists between such neuron pairs. Since single cortical neurons show

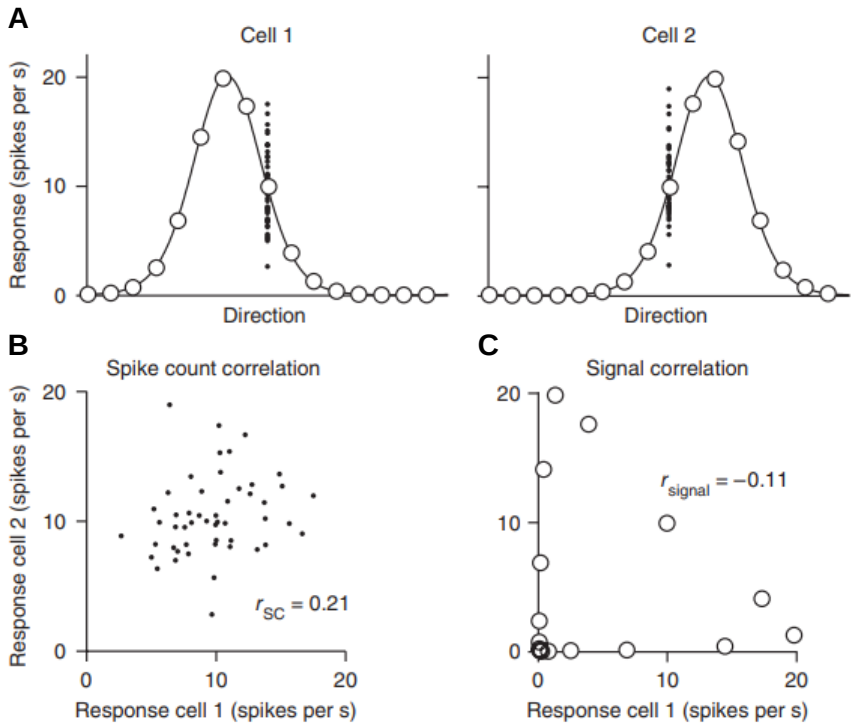

Figure 4. Illustration of signal and spike count (aka noise) correlation. (A) Two sample neurons showing different tuning curves and different trial-by-trial variability given the same stimulus. Large circles are averaged response to the particular stimulus. (B) Scatter plot of cell1 and 2 responses evoked by the same stimulus, the spike count correlation is calculated as the Pearson correlation coefficient of the data. (C) Scatter plot of the averaged responses of cell 1 and 2 for all stimuli. (Cohen and Kohn, 2011)

unreliable responses to repeated presentation of an identical stimulus, there is significant trial-to-trial fluctuation around the mean response. The amount of fluctuation shared by pairs of neurons can be quantified using “noise” correlation. Therefore, noise correlation measures the degree of trial-by-trial firing differences between two neurons without considering their preference on each sensory stimulus (Figure 4B).

Altered bottom-up inputs that shift tuning curves of the excitatory neurons could cause changes in signal and noise correlations. Top-down modifications from higher

order cortices or the motor cortex could also influence the noise correlation (Bondy et al., 2018). Although it is important to investigate underlying mechanisms that alter the interactions between neuron pairs, this is beyond the scope of the current thesis. My thesis aims to identify the change in correlation structure that associates performance improvement during learning.

1.1.7 The Effects of Noise Correlation on the Amount of Encoded Information

A key question is whether and how noise correlation influences the encoding capacity of a neuron population. In other words, does noise correlation increase or decrease the amount of information encoded by neuronal populations A dogmatic view in the field posits that correlated noise will decrease the amount of sensory information encoded by the neuron population (Adibi et al., 2013; Bartolo et al., 2020; Chen et al., 2015; Kafashan et al., 2021; Petersen et al., 2001; Rumyantsev et al., 2020; Sanayei et al., 2018; Tremblay et al., 2015). Because cortical neurons respond unreliably with tremendous amounts of noise, utilizing population average responses will cancel out the unwanted noise and improve the fidelity of signal representation. However, if noises are correlated, [the?] population code fails to improve the signal-to-noise ratio, therefore decreasing the amount of information encoded.

The key to understanding the role of noise correlation is to measure its change during or after learning. Some previous studies reported that learning increases noise correlation while others reported a decrease. The contradictory result may be due to oversimplified quantification of noise correlation as a single value averaged across the whole population. In fact, noise correlation should be measured together with signal correlation to reveal their function in sensory learning.

When considering representation of sensory stimulus by a neuronal population, we want to first set up a high dimensional space of neuronal activity, in which each axis measures the intensity of a single neuron's activity. For each trial, the vector of neuron population activity is a dot in this high dimensional space with its coordinates composed by individual neuronal activity. Because of the variances of cortical neural responses, the dots of population activities in response to a repetitive stimulus form a cluster. The ability of encoding and discriminating two distinct sensory stimuli relies on the degree of overlapping between two clusters of population codes in the activity space. If the signal correlation of a neuron pair is positive (i.e. similar tuning curves), a positive noise correlation will result in a greater overlap between the two activity clouds than if there were no correlation, decreasing the amount of information possibly encoded. The two stimuli are represented similarly and potentially generalized. The same conclusion applies when signal and noise correlations are both negative. On the contrary, if signal and noise correlations have different signs, the overlap between two activity clouds becomes smaller, increasing the amount of information encoded. In other words, two stimuli are represented more distinctively, and the decision boundary is easier to draw.

Besides the encoding efficiency, the activity of the primary sensory cortex will have to be read out by its downstream area eventually. Discussing the effect of noise correlation on the amount of propagated information is also important. Conventionally, a linear readout scheme is assumed for a population, and correlated neural activity seems to be redundant and decreases the coding efficiency. However, in the brain, the network is often equipped to solve various problems and stay flexible in coding. Computational studies explored a nonlinear readout scheme which considers the higher-order statistics

of a correlated neuron population, and found out that noise correlation does not limit the growth of encoded information as the population grows in size. (Shamir and Sompolinsky, 2004).

1.2 Cortical Plasticity and Learning

1.2.1 Methods to Probe Learning-Induced Cortical Plasticity

While stimulus-evoked activities in L4 neurons are stable, neurons in L2/3 exhibit task-dependent plasticity of their activities during sensory learning, even in adult brains. During learning, a specific sensory cue or context can be associated with a particular behavioral output. To reinforce this association, animals are often given a reward when they exhibit correct behavioral responses. In wS1, the first stage of cortical processing of whisker input, the neuronal representations of sensory stimuli undergo learning-induced modifications. These changes are thought to amplify task-related sensory signals and facilitate the transmission of task-relevant sensory signals to downstream areas where they are used to drive appropriate behavioral responses.

To examine the effects of learning on population activity in the sensory cortex, researchers often train mice to perform sensory learning tasks while monitoring the population activity using various *in vivo* recording methods. This approach facilitates the identification of quantitative relationships between neural activity and behavioral performance. Many different whisker-guided tactile tasks have been used in the field. Experimenters are able to systematically vary different parameters of whisker stimulation including the amplitude, frequency or orientation. Advanced recording techniques, such as two-photon calcium imaging and *in vivo* multi-electrode recordings, are used to measure neuronal activity as animals perform the task. These methods can

be combined with optogenetic and/or chemogenetic manipulations for testing causal contribution of population activities.

1.2.2 Single Neuron Plasticity

A common strategy for the brain to learn both detection and discrimination tasks involves selective potentiation of neural responses to reward-associated stimulus features. Neuronal tuning curves can undergo different types of changes. These include shift and/or expansion that result in representation of preferred feature (Goltstein et al., 2013; Reed et al., 2011), and sharpening of tuning curves resulting in better separation of different features (Schoups et al., 2001; Yang and Maunsell, 2004). Indeed, many studies comparing the neuron activity before and after sensory learning reported amplified responses and prolonged recurrent neuron activity to the rewarded stimuli after learning. In addition, sensory familiarization, without the association of rewards or punishment, reduces the population response that leads to sharpening of the tuning curve (Freedman et al., 2006; Meyer et al., 2014; Woloszyn and Sheinberg, 2012). Photo-inactivation of the potentiated activity reduces the hit rate (i.e. the percentage of correct trials in ‘Go’ trials in one training session) of animal performance, suggesting a causal relationship between elevated neural activity and improvement in signal detection. In contrast, repetitive exposure of the same sensory stimulus without an associative reward leads to decreases of neural responses in primary sensory cortices towards such stimulus (Henschke et al., 2020; Keller et al., 2017; Rabinovich et al., 2022). The reduction of responses toward unrewarded stimuli could serve as alternative mechanisms of tuning curve sharpening and shifting.

Cortical INs are thought to mediate various aspects of learning-induced modifications in the circuit through inhibition and disinhibition. At a high level, GABAergic INs that closely synapse with pyramidal neurons serve as a gate for dendritic integration, so lifting the inhibition should allow coincidental inputs to combine and drive plasticity to enhance the population response towards certain stimulus. For instance, it is proposed that stimulus-tuned SST INs selectively disinhibit similarly tuned pyramidal neurons through inhibiting PV INs, allowing the excitatory plasticity to recruit more pyramidal neurons responding to such stimulus (Wilmes and Clopath, 2019). The key questions are what INs inhibit PV neurons and what is the source of input. One emerging theory suggests two-step plasticity for a VIP-SST-PV-PYR cortical L2/3 microcircuit to gain responsiveness to a rewarded stimulus. Firstly, the reward-mediated top-down input activates VIP neurons which in turn inhibit SST neurons following a transient activation of SST through sensory stimulus presentation. SST inhibition leads to disinhibited PV neurons, which increase the firing rate of PV neurons. According to spike-timing-dependent plasticity of inhibitory synapses, the brief excitation of SST neurons followed by PV firing strengthens the SST-PV synapses (Wilmes and Clopath, 2019). Therefore, the reward information is now represented by selectively strengthened inhibitory SST-PV projection. In expert animals, even when the reward is absent, the presentation of reward-associated sensory stimulus will activate SST INs, inhibit PV Ins, and disinhibit PYR neurons, leading to potentiation of the projections from rewarded PYR to the remaining PYR. As a result, the excitatory neuron population in L2/3 generates a stronger collective response towards rewarded signals (Wilmes and Clopath, 2019). VIP neurons receive multiple top-down inputs including reward signals.

In vivo electrode recording discovered that the activity of VIP neurons A1 correlates with the timing of reward/punishment, suggesting rewarding status could be another source of inputs to VIP neurons and drive the plasticity in primary sensory cortex (Pi et al., 2013).

Taken together, learning enhances representation of task-relevant sensory stimuli in L2/3 neurons of wS1 by increasing their sensitivity, and this learning-induced potentiation plays a causal role in stimulus detection.

In addition to increasing the sensitivity of task-related sensory stimuli, improving the ability to differentiate between stimuli is also crucial for learning sensorimotor tasks. This requires conversion of a continuous spectrum of variable stimulus features into discrete categories. One potential mechanism involves representing stimulus categories using a subset of neurons that have the ability to broaden their tuning curve within each category. For example, a study in the mouse A1 found categorical neurons that respond not only to a specific auditory tone but also to a range of auditory pitches (Xin et al., 2019). Furthermore, the cutoff of neuronal responses aligned with the behavioral boundary instructed in the task and was adaptive to shifts in the boundary, suggesting that these neurons play a role in categorizing stimuli into distinct groups.

1.2.3 Population Coding Plasticity

A separate line of investigation has focused on learning-induced modifications in coding at the neuronal population level. These studies have reported the formation and functions of neuron ensembles in representing task-related stimuli during learning (Holtmaat and Caroni, 2016). By recruiting neurons into distinct functional ensembles depending on stimulus feature selectivity, the neuronal population could acquire the

ability to represent stimulus categories. These ensembles potentially target different neuronal subpopulations in a category-specific manner, thus transmitting category-related signals to the downstream areas. Mechanisms underlying the emergence of categorical ensembles within the primary sensory cortex are still unclear.

Many of the observed plasticity mechanisms require task engagement for their expression, as they are not observed in animals under anesthesia or in disengaged/satiated states. Such state dependency indicates that plasticity may not be based on local synaptic connections within the sensory cortex but likely requires top-down modulation by long-range projections during task engagement.

1.2.4 Changes in Noise Correlation as a Function of Learning or Experiences

Theoretically, noise correlation is thought to limit the sensory encoding capacity in a neuron population, which would decrease the accuracy of trial-to-trial population representation and impair sensory detection or discrimination of sensory input during task performance (Averbeck et al., 2006; Cohen and Kohn, 2011; Rumyantsev et al., 2020; Zohary et al., 1994). However, both the decrease and increase of noise correlation as a result of learning were observed in experiments (Jeanne et al., 2013; Khan et al., 2018; Kwon et al., 2016; Ni et al., 2018). Although noise correlation could cause redundancy that limits the encoding capacity of the neuron population, correlated responses within a functional subset of neurons could also benefit discrimination between sensory stimuli and/or facilitate sensory information readout (Safaai et al., 2013). A key step toward resolving these discrepancies and to understand the benefits and limits of noise correlations is to investigate the “structure” of noise correlation. This involves quantifying neuronal correlations as a function of the tuning properties of

individual neurons and testing whether the correlated activity is better for the task performance than their independent activities.

Electrophysiological recording in songbird Caudolateral Mesopallium, a higher-order auditory cortex encoding complex motifs of songs, showed that associative learning selectively alters the correlations between neuron pairs that are tuned to the task-relevant stimuli (Jeanne et al., 2013). Specifically, the lowest noise correlation was found between neuron pairs tuned to similar song motifs while high noise correlation was found in neuron pairs tuned to distinct motifs (Jeanne et al., 2013). This finding supports the theory that the structure of noise correlation is a target of changes during sensory associative learning and its change may lead to functional improvement. This study includes a comparative analysis that uses a multinomial logistic regression method to find a classifier that is well-suited for motif identification to assess the decoding capability of neural input with or without learning-altered noise correlation (Jeanne et al., 2013). The results demonstrate superior performance when the preserved noise correlation is opposing signal correlation. In addition, other studies support that the structure of noise correlation changes dynamically depending on task instruction rather than remaining fixed to sensory features (Bondy et al., 2018; Cohen and Newsome, 2008), indicating that changes in noise correlation positively contribute to learning in sensory cortices in mammals. These results argue that the limiting effect on sensory encoding does not apply to the learning-dependent reconstruction of noise correlation.

1.2.5 Noise Correlation Facilitates Signal Transmission through Increasing Encoding Consistency

The ultimate purpose of encoding sensory signals is to propagate to other brain regions and generate appropriate behavior. Noise correlation can facilitate this propagation by increasing response reliability (Cafaro and Rieke, 2010). This potentially increases the probability of spike generations by promoting the temporal integration of synaptic inputs (Panzeri et al., 2022; Reyes, 2003). Indeed, studies demonstrate that spike generation is enhanced when input spikes are spatially and temporally correlated (Diesmann et al., 1999; Zandvakili and Kohn, 2015). Furthermore, coincident events at dendrites could trigger plasticity at the connecting synapses, which may be the underlying mechanisms of V1 orientation tuning and grid cell firing. These studies laid the biophysical foundation for the role of noise correlations in propagating sensory signals to downstream areas. Evidence supporting this notion is found in studies showing that convergence feedforward networks trigger more selective and reliable postsynaptic responses even when the inputs are correlated and information is limited (Ackels et al., 2021; Valente et al., 2021; Zylberberg et al., 2017). These results

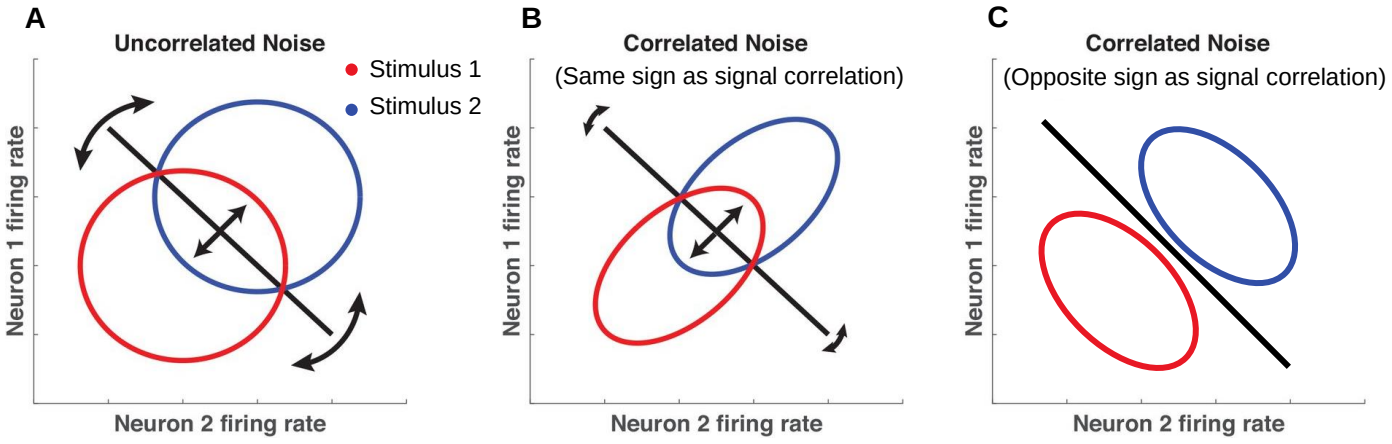

Figure 5. The effect of correlated noise on decision boundary. (A) Two neurons with uncorrelated noise have high percentage overlap of blue (stimulus 1) and red (stimulus 1) activity, causing huge boundary (solid black line) adjustment along irrelevant dimensions (double-arrow curves indicating the rotation of solid line). (Nassar et al., 2021) (B) Correlated noise between two similarly tuned neurons, resulting the plane of neuronal activity orthogonal to the optimal decision boundary. This will help maximizing the boundary adjustment along relevant dimension (double-arrow dash in the middle of solid line). (Nassar et al., 2021)(C) Modified to illustrate when correlated noise has opposite sign as signal correlation, overlaps between red and blue activity may be minimized. (Averbeck et al., 2006)

emphasize the role of noise correlation in improving readout efficacy which questions the necessity of maximizing sensory encoding capacity.

Theoretical studies argue that the behavioral boundary made by the animals could be optimized by correlated noise (Figure 5) (Averbeck et al., 2006; Nassar et al., 2021). As figure 5B shows, correlated noise not only reduces the overlap between two neuronal activity clouds, but also limits the range of rotation of the decision boundary, benefiting discrimination of the neuronal representation of two stimuli. Moreover, figure 5C demonstrates that when correlated noise has an opposite sign from the correlated tuning curve, the overlap is minimized. A study in PPC reported stronger noise correlation among neuron pairs that are tuned to similar sensory motifs, suggesting their enhancing role in readout during sensory discrimination tasks. However, there has been no study exploring the structure of noise correlation in the primary sensory cortex in the context of sensory discrimination. My thesis research will fill in the gap by imaging neurons in the mouse wS1 while the animal is performing whisker-involved discrimination tasks.

1.2.6 Structures of Noise Correlation and Synaptic Connection

The underlying mechanisms that give rise to neuronal correlations are being revealed. Theoretical and experimental studies have proposed various sources for noise correlation, such as top-down input from higher-order cortical areas modulation, shared similar bottom-up input, and neuromodulatory inputs reflecting behavioral states.

Studies utilizing *in vivo* calcium imaging in conjunction with brain slice recording of the same cells reported that the probability of synaptic connections between highly correlated excitatory neurons is greater, elucidating synaptic connection in one of the

sources of noise correlation. Synaptic plasticity is initiated in cortical circuits during sensory associative learning. Computational neuroscientists have proposed two-step learning induced plasticity in the microcircuit model of the V1 cortical network. The two-step plasticity begins with the potentiation of responses in SST INs tuned toward rewarded stimuli, which then drives the strengthening of selective synaptic projections that recruit more pyramidal neurons to respond to the task-relevant stimulus. The noise correlation among the excitatory neurons selectively increased after the phase two of plasticity. This result led to the hypothesis that structured synaptic strengthening causes the structured noise correlations.

1.3 Specific Aims

1.3.1 Overarching Hypothesis

Perception involves the representation of external sensory stimuli by a neuron population and the propagation of task-relevant activities to appropriate downstream areas to generate appropriate behaviors. Neuronal correlation is thought to have negative impacts on the sensory representation but positive impact on the propagation. Whether the net effect of noise correlations does more good than harm to the brain's ability to carry out sensorimotor computation is highly debatable. Most prior studies have focused on its limiting effects in sensory encoding. More recently, potential advantages of structured increases in noise correlation – such as enhanced propagation of task-relevant signals - are being increasingly recognized.

Although theoretical works have considered both information-limiting and propagation-enhancing effects of noise correlation, very few studies have measured the "structure" of noise correlations, the correlation matrix as a function of neuronal tuning.

Without this measurement, the full landscape of learning-induced changes in noise correlations cannot be captured, which severely limits our understanding of cortical plasticity mechanisms. The paucity of empirical data results from the difficulty of monitoring large neuron populations with high resolution in task-performing animals. Another important caveat from prior studies is the lack of negative controls in which animals are passively exposed to the stimuli presented.

Using *in vivo* population imaging and sophisticated behavioral tasks, I probe learning-induced modifications of noise correlation structures in wS1. I hypothesize that learning increases category-specific neuronal correlations in the primary sensory cortex.

1.3.2 Specific Aim #1: Characterize the Structure and Function of Noise Correlation in Primary Somatosensory Cortex During Sensory Associative Learning

Comparison of the structure of neuronal correlations before and after learning will elucidate how they change during sensory-associative learning and how such change impacts encoding of sensory information. I tested the specific hypothesis that the noise correlation will increase among similarly tuned neuron pairs through learning despite its limiting effect on sensory encoding fidelity.

To effectively assess the structure of noise correlation in the context of neuronal tuning properties, I designed a whisker discrimination task with nine different deflective frequencies to characterize the in-task tuning curve of individual neurons. Animals learned to categorize deflection frequencies into two groups that are associated with distinct behaviors. The structure of noise correlation was extracted from population

imaging of wS1 L2/3 GCaMP-expressing neurons as a correlation matrix sorted by neuronal tuning.

To test whether the noise correlation in expert mice exerts “information-limiting” effects as predicted by prior work, I compared the accuracy of decoding stimulus categories using original data and correlation-free data. To dissociate the population activity from pairwise noise correlation, I shuffled the individual data across trials to disrupt the tuning-independent correlations. The analysis employed a supervised machine-learning method to train a classifier based on the input of population data. The predictive power of such a classifier in categorizing the two stimuli groups indicates the amount of information encoded by the population activity. If the classifier on correlation-free data shows a higher test score than the one on original data, then I would conclude that the noise correlation reduces the amount of information encoded.

Lastly, to advance understanding on the emergence of the noise correlation, the same series of analyses were carried out in a task-disengaged state.

1.3.3 Specific Aim #2: Test Task-Specificity of Noise Correlation Changes

Cortical plasticity processes could vary depending on specific task rules such as detection, discrimination, categorization, etc. We know little about the generality of learning-induced changes across different tasks. For example, learning-induced changes that facilitate the classification of stimuli into two groups in one task may introduce unwanted selectivity at the boundary, which may compromise performance in a detection task. To gain further insights into their role in different tasks, I tested if patterns of changes in neuronal correlations are conserved across different tasks or not by comparing them under two different tasks – discrimination versus detection. Based

on prior work showing that noise-correlations are modulated by top-down input, I hypothesize that, depending on the task, highly correlated neuron pairs would show co-tuning to different sets of stimuli.

1.4 References

Abraira, V.E., and Ginty, D.D. (2013). The sensory neurons of touch. Neuron 79, 618-639.

Ackels, T., Erskine, A., Dasgupta, D., Marin, A.C., Warner, T.P., Tootoonian, S., Fukunaga, I., Harris, J.J., and Schaefer, A.T. (2021). Fast odour dynamics are encoded in the olfactory system and guide behaviour. Nature 593, 558-563.

Adibi, M., McDonald, J.S., Clifford, C.W., and Arabzadeh, E. (2013). Adaptation improves neural coding efficiency despite increasing correlations in variability. Journal of Neuroscience 33, 2108-2120.

Allen, C.B., Celikel, T., and Feldman, D.E. (2003). Long-term depression induced by sensory deprivation during cortical map plasticity in vivo. Nature neuroscience 6, 291-299.

Averbeck, B.B., Latham, P.E., and Pouget, A. (2006). Neural correlations, population coding and computation. Nature reviews neuroscience 7, 358-366.

Banerjee, A., Parente, G., Teutsch, J., Lewis, C., Voigt, F.F., and Helmchen, F. (2020). Value-guided remapping of sensory cortex by lateral orbitofrontal cortex. Nature 585, 245-250.

Barak, O., Rigotti, M., and Fusi, S. (2013). The sparseness of mixed selectivity neurons controls the generalization–discrimination trade-off. Journal of Neuroscience 33, 3844-3856.

Barth, A.L., and Poulet, J.F. (2012). Experimental evidence for sparse firing in the neocortex. Trends in neurosciences 35, 345-355.

Bartolo, R., Saunders, R.C., Mitz, A.R., and Averbeck, B.B. (2020). Information-limiting correlations in large neural populations. Journal of Neuroscience 40, 1668-1678.

Beyeler, M., Rounds, E.L., Carlson, K.D., Dutt, N., and Krichmar, J.L. (2019). Neural correlates of sparse coding and dimensionality reduction. PLoS computational biology 15, e1006908.

Bondy, A.G., Haefner, R.M., and Cumming, B.G. (2018). Feedback determines the structure of correlated variability in primary visual cortex. Nature neuroscience 21, 598-606.

Cafaro, J., and Rieke, F. (2010). Noise correlations improve response fidelity and stimulus encoding. Nature 468, 964-967.

Chen, J.L., Carta, S., Soldado-Magraner, J., Schneider, B.L., and Helmchen, F. (2013). Behaviour-dependent recruitment of long-range projection neurons in somatosensory cortex. Nature 499, 336-340.

Chen, Q., Deister, C.A., Gao, X., Guo, B., Lynn-Jones, T., Chen, N., Wells, M.F., Liu, R., Goard, M.J., and Dimidschstein, J. (2020). Dysfunction of cortical GABAergic neurons leads to sensory hyper-reactivity in a Shank3 mouse model of ASD. Nature neuroscience 23, 520-532.

Chen, Y.-p., Lin, C.-p., Hsu, Y.-c., and Hung, C.P. (2015). Network anisotropy trumps noise for efficient object coding in macaque inferior temporal cortex. Journal of Neuroscience 35, 9889-9899.

Clancy, K.B., Koralek, A.C., Costa, R.M., Feldman, D.E., and Carmena, J.M. (2014). Volitional modulation of optically recorded calcium signals during neuroprosthetic learning. Nature neuroscience 17, 807-809.

Cohen, M.R., and Kohn, A. (2011). Measuring and interpreting neuronal correlations. Nature neuroscience 14, 811-819.

Cohen, M.R., and Newsome, W.T. (2008). Context-dependent changes in functional circuitry in visual area MT. Neuron 60, 162-173.

Cornford, J.H., Mercier, M.S., Leite, M., Magloire, V., Häusser, M., and Kullmann, D.M. (2019). Dendritic NMDA receptors in parvalbumin neurons enable strong and stable neuronal assemblies. Elife 8, e49872.

Cossell, L., Iacaruso, M.F., Muir, D.R., Houlton, R., Sader, E.N., Ko, H., Hofer, S.B., and Mrsic-Flogel, T.D. (2015). Functional organization of excitatory synaptic strength in primary visual cortex. Nature 518, 399-403.

Coste, B., Mathur, J., Schmidt, M., Earley, T.J., Ranade, S., Petrus, M.J., Dubin, A.E., and Patapoutian, A. (2010). Piezo1 and Piezo2 are essential components of distinct mechanically activated cation channels. Science 330, 55-60.

Crochet, S., Poulet, J.F., Kremer, Y., and Petersen, C.C. (2011). Synaptic mechanisms underlying sparse coding of active touch. Neuron 69, 1160-1175.

Dalgleish, H.W., Russell, L.E., Packer, A.M., Roth, A., Gauld, O.M., Greenstreet, F., Thompson, E.J., and Häusser, M. (2020). How many neurons are sufficient for perception of cortical activity? Elife 9, e58889.

de Lafuente, V., and Romo, R. (2005). Neuronal correlates of subjective sensory experience. Nature neuroscience 8, 1698-1703.

de Lafuente, V., and Romo, R. (2006). Neural correlate of subjective sensory experience gradually builds up across cortical areas. Proceedings of the National Academy of Sciences 103, 14266-14271.

Diesmann, M., Gewaltig, M.-O., and Aertsen, A. (1999). Stable propagation of synchronous spiking in cortical neural networks. Nature 402, 529-533.

Doron, G., Shin, J.N., Takahashi, N., Drüke, M., Bocklisch, C., Skenderi, S., de Mont, L., Toumazou, M., Ledderose, J., and Brecht, M. (2020). Perirhinal input to neocortical layer 1 controls learning. Science 370, eaaz3136.

Ecker, A.S., Berens, P., Keliris, G.A., Bethge, M., Logothetis, N.K., and Tolias, A.S. (2010). Decorrelated neuronal firing in cortical microcircuits. science 327, 584-587.

Erzurumlu, R.S., Bates, C.A., and Killackey, H.P. (1980). Differential organization of thalamic projection cells in the brain stem trigeminal complex of the rat. Brain research 198, 427-433.

Erzurumlu, R.S., and Killackey, H.P. (1979). Efferent connections of the brainstem trigeminal complex with the facial nucleus of the rat. Journal of Comparative Neurology 188, 75-86.

Esmaeili, V., Oryshchuk, A., Asri, R., Tamura, K., Foustoukos, G., Liu, Y., Guiet, R., Crochet, S., and Petersen, C.C. (2022). Learning-related congruent and incongruent changes of excitation and inhibition in distinct cortical areas. PLoS Biology 20, e3001667.

Esmaeili, V., Tamura, K., Foustoukos, G., Oryshchuk, A., Crochet, S., and Petersen, C.C. (2020). Cortical circuits for transforming whisker sensation into goal-directed licking. Current Opinion in Neurobiology 65, 38-48.

Feldman, D.E. (2000). Timing-based LTP and LTD at vertical inputs to layer II/III pyramidal cells in rat barrel cortex. Neuron 27, 45-56.

Feldman, D.E., and Brecht, M. (2005). Map plasticity in somatosensory cortex. Science 310, 810-815.

Freedman, D.J., Riesenhuber, M., Poggio, T., and Miller, E.K. (2006). Experience-dependent sharpening of visual shape selectivity in inferior temporal cortex. Cerebral Cortex 16, 1631-1644.

Fukuda, T. (2017). Structural organization of the dendritic reticulum linked by gap junctions in layer 4 of the visual cortex. Neuroscience 340, 76-90.

Fukuda, T., Kosaka, T., Singer, W., and Galuske, R.A. (2006). Gap junctions among dendrites of cortical GABAergic neurons establish a dense and widespread intercolumnar network. Journal of Neuroscience 26, 3434-3443.

Gawne, T.J., and Richmond, B.J. (1993). How independent are the messages carried by adjacent inferior temporal cortical neurons? Journal of Neuroscience 13, 2758-2771.

Goltstein, P.M., Coffey, E.B., Roelfsema, P.R., and Pennartz, C.M. (2013). In vivo two-photon Ca2+ imaging reveals selective reward effects on stimulus-specific assemblies in mouse visual cortex. Journal of Neuroscience 33, 11540-11555.

Haeberle, H., and Lumpkin, E.A. (2008). Merkel cells in somatosensation. Chemosensory perception 1, 110-118.

Hatch, R.J., Mendis, G.D.C., Kaila, K., Reid, C.A., and Petrou, S. (2017). Gap junctions link regular-spiking and fast-spiking interneurons in layer 5 somatosensory cortex. Frontiers in Cellular Neuroscience 11, 204.

Henschke, J.U., Dylda, E., Katsanevaki, D., Dupuy, N., Currie, S.P., Amvrosiadis, T., Pakan, J.M., and Rochefort, N.L. (2020). Reward association enhances stimulus-specific representations in primary visual cortex. Current Biology 30, 1866-1880. e1865.

Hestrin, S., and Galarreta, M. (2005). Electrical synapses define networks of neocortical GABAergic neurons. Trends in neurosciences 28, 304-309.

Hoffman, B.U., Baba, Y., Griffith, T.N., Mosharov, E.V., Woo, S.-H., Roybal, D.D., Karsenty, G., Patapoutian, A., Sulzer, D., and Lumpkin, E.A. (2018). Merkel cells activate sensory neural pathways through adrenergic synapses. Neuron 100, 1401-1413. e1406.

Holtmaat, A., and Caroni, P. (2016). Functional and structural underpinnings of neuronal assembly formation in learning. Nature neuroscience 19, 1553-1562.

House, D.R., Elstrott, J., Koh, E., Chung, J., and Feldman, D.E. (2011). Parallel regulation of feedforward inhibition and excitation during whisker map plasticity. Neuron 72, 819-831.

Houweling, A.R., and Brecht, M. (2008). Behavioural report of single neuron stimulation in somatosensory cortex. Nature 451, 65-68.

Jeanne, J.M., Sharpee, T.O., and Gentner, T.Q. (2013). Associative learning enhances population coding by inverting interneuronal correlation patterns. Neuron 78, 352-363.

Jensen, K.F., and Killackey, H.P. (1987). Terminal arbors of axons projecting to the somatosensory cortex of the adult rat. I. The normal morphology of specific thalamocortical afferents. Journal of Neuroscience 7, 3529-3543.

Kafashan, M., Jaffe, A.W., Chettih, S.N., Nogueira, R., Arandia-Romero, I., Harvey, C.D., Moreno-Bote, R., and Drugowitsch, J. (2021). Scaling of sensory information in large neural populations shows signatures of information-limiting correlations. Nature communications 12, 473.

Keller, A.J., Houlton, R., Kampa, B.M., Lesica, N.A., Mrsic-Flogel, T.D., Keller, G.B., and Helmchen, F. (2017). Stimulus relevance modulates contrast adaptation in visual cortex. Elife 6, e21589.

Khan, A.G., Poort, J., Chadwick, A., Blot, A., Sahani, M., Mrsic-Flogel, T.D., and Hofer, S.B. (2018). Distinct learning-induced changes in stimulus selectivity and interactions of GABAergic interneuron classes in visual cortex. Nature neuroscience 21, 851-859.

Killackey, H.P. (1973). Anatomical evidence for cortical subdivisions based on vertically discrete thalamic projections from the ventral posterior nucleus to cortical barrels in the rat. Brain research 51, 326-331.

Kinnischtzke, A.K., Fanselow, E.E., and Simons, D.J. (2016). Target-specific M1 inputs to infragranular S1 pyramidal neurons. Journal of neurophysiology 116, 1261-1274.

Kinnischtzke, A.K., Simons, D.J., and Fanselow, E.E. (2014). Motor cortex broadly engages excitatory and inhibitory neurons in somatosensory barrel cortex. Cerebral cortex 24, 2237-2248.

Ko, H., Hofer, S.B., Pichler, B., Buchanan, K.A., Sjöström, P.J., and Mrsic-Flogel, T.D. (2011). Functional specificity of local synaptic connections in neocortical networks. Nature 473, 87-91.

Koerber, H.R., and Woodbury, C.J. (2002). Comprehensive phenotyping of sensory neurons using an ex vivo somatosensory system. Physiology & behavior 77, 589-594.

Kwon, S.E., Yang, H., Minamisawa, G., and O'Connor, D.H. (2016). Sensory and decision-related activity propagate in a cortical feedback loop during touch perception. Nature neuroscience 19, 1243-1249.

Lee, S., Kruglikov, I., Huang, Z.J., Fishell, G., and Rudy, B. (2013). A disinhibitory circuit mediates motor integration in the somatosensory cortex. Nature neuroscience 16, 1662-1670.

Lee, T., Alloway, K.D., and Kim, U. (2011). Interconnected cortical networks between primary somatosensory cortex septal columns and posterior parietal cortex in rat. Journal of Comparative Neurology 519, 405-419.

Li, C., and Bak, A. (1976). Excitability characteristics of the A-and C-fibers in a peripheral nerve. Experimental neurology 50, 67-79.

Liu, D., Deng, J., Zhang, Z., Zhang, Z.-Y., Sun, Y.-G., Yang, T., and Yao, H. (2020). Orbitofrontal control of visual cortex gain promotes visual associative learning. Nature communications 11, 2784.

Lo, F.-S., Guido, W., and Erzurumlu, R.S. (1999). Electrophysiological properties and synaptic responses of cells in the trigeminal principal sensory nucleus of postnatal rats. Journal of neurophysiology 82, 2765-2775.

Manita, S., Suzuki, T., Homma, C., Matsumoto, T., Odagawa, M., Yamada, K., Ota, K., Matsubara, C., Inutsuka, A., and Sato, M. (2015). A top-down cortical circuit for accurate sensory perception. Neuron 86, 1304-1316.

Marshel, J.H., Kim, Y.S., Machado, T.A., Quirin, S., Benson, B., Kadmon, J., Raja, C., Chibukhchyan, A., Ramakrishnan, C., and Inoue, M. (2019). Cortical layer–specific critical dynamics triggering perception. Science 365, eaaw5202.

Melzack, R., and Wall, P.D. (1962). On the nature of cutaneous sensory mechanisms. Brain 85, 331-356.

Merkel, F. (1875). Tastzellen und Tastkörperchen bei den Hausthieren und beim Menschen. Archiv für mikroskopische Anatomie 11, 636-652.

Meyer, T., Walker, C., Cho, R.Y., and Olson, C.R. (2014). Image familiarization sharpens response dynamics of neurons in inferotemporal cortex. Nature neuroscience 17, 1388-1394.

Minamisawa, G., Kwon, S.E., Chevée, M., Brown, S.P., and O'Connor, D.H. (2018). A non-canonical feedback circuit for rapid interactions between somatosensory cortices. Cell reports 23, 2718-2731. e2716.

Mohan, H., de Haan, R., Broersen, R., Pieneman, A.W., Helmchen, F., Staiger, J.F., Mansvelder, H.D., and de Kock, C.P. (2019). Functional architecture and encoding of tactile sensorimotor behavior in rat posterior parietal cortex. Journal of Neuroscience 39, 7332-7343.

Nassar, M.R., Scott, D., and Bhandari, A. (2021). Noise correlations for faster and more robust learning. Journal of Neuroscience 41, 6740-6752.

Ni, A.M., Ruff, D.A., Alberts, J.J., Symmonds, J., and Cohen, M.R. (2018). Learning and attention reveal a general relationship between population activity and behavior. Science 359, 463-465.

Panzeri, S., Macke, J.H., Gross, J., and Kayser, C. (2015). Neural population coding: combining insights from microscopic and mass signals. Trends in cognitive sciences 19, 162-172.

Panzeri, S., Moroni, M., Safaai, H., and Harvey, C.D. (2022). The structures and functions of correlations in neural population codes. Nature Reviews Neuroscience 23, 551-567.

Peron, S., Pancholi, R., Voelcker, B., Wittenbach, J.D., Ólafsdóttir, H.F., Freeman, J., and Svoboda, K. (2020). Recurrent interactions in local cortical circuits. Nature 579, 256-259.

Petersen, C.C. (2019). Sensorimotor processing in the rodent barrel cortex. Nature Reviews Neuroscience 20, 533-546.

Petersen, C.C., Hahn, T.T., Mehta, M., Grinvald, A., and Sakmann, B. (2003). Interaction of sensory responses with spontaneous depolarization in layer 2/3 barrel cortex. Proceedings of the National Academy of Sciences 100, 13638-13643.

Petersen, R.S., Panzeri, S., and Diamond, M.E. (2001). Population coding of stimulus location in rat somatosensory cortex. Neuron 32, 503-514.

Pfeffer, C.K., Xue, M., He, M., Huang, Z.J., and Scanziani, M. (2013). Inhibition of inhibition in visual cortex: the logic of connections between molecularly distinct interneurons. Nature neuroscience 16, 1068-1076.

Pi, H.-J., Hangya, B., Kvitsiani, D., Sanders, J.I., Huang, Z.J., and Kepecs, A. (2013). Cortical interneurons that specialize in disinhibitory control. Nature 503, 521-524.

Rabinovich, R.J., Kato, D.D., and Bruno, R.M. (2022). Learning enhances encoding of time and temporal surprise in mouse primary sensory cortex. Nature Communications 13, 5504.

Ranjbar-Slamloo, Y., and Arabzadeh, E. (2019). Diverse tuning underlies sparse activity in layer 2/3 vibrissal cortex of awake mice. The Journal of Physiology 597, 2803-2817.

Reed, A., Riley, J., Carraway, R., Carrasco, A., Perez, C., Jakkamsetti, V., and Kilgard, M.P. (2011). Cortical map plasticity improves learning but is not necessary for improved performance. Neuron 70, 121-131.

Reyes, A.D. (2003). Synchrony-dependent propagation of firing rate in iteratively constructed networks in vitro. Nature neuroscience 6, 593-599.

Rinberg, D., Koulakov, A., and Gelperin, A. (2006). Sparse odor coding in awake behaving mice. Journal of Neuroscience 26, 8857-8865.

Rumyantsev, O.I., Lecoq, J.A., Hernandez, O., Zhang, Y., Savall, J., Chrapkiewicz, R., Li, J., Zeng, H., Ganguli, S., and Schnitzer, M.J. (2020). Fundamental bounds on the fidelity of sensory cortical coding. Nature 580, 100-105.

Sachidhanandam, S., Sermet, B.S., and Petersen, C.C. (2016). Parvalbumin-expressing GABAergic neurons in mouse barrel cortex contribute to gating a goal-directed sensorimotor transformation. Cell reports 15, 700-706.

Safaai, H., von Heimendahl, M., Sorando, J.M., Diamond, M.E., and Maravall, M. (2013). Coordinated population activity underlying texture discrimination in rat barrel cortex. Journal of Neuroscience 33, 5843-5855.

Sanayei, M., Chen, X., Chicharro, D., Distler, C., Panzeri, S., and Thiele, A. (2018). Perceptual learning of fine contrast discrimination changes neuronal tuning and population coding in macaque V4. Nature communications 9, 4238.

Schneider, D.M., Sundararajan, J., and Mooney, R. (2018). A cortical filter that learns to suppress the acoustic consequences of movement. Nature 561, 391-395.

Schoups, A., Vogels, R., Qian, N., and Orban, G. (2001). Practising orientation identification improves orientation coding in V1 neurons. Nature 412, 549-553.

Schreiner, R., Essick, G., and Whitsel, B. (1978). Variability in somatosensory cortical neuron discharge: effects on capacity to signal different stimulus conditions using a mean rate code. Journal of Neurophysiology 41, 338-349.

Shamir, M., and Sompolinsky, H. (2004). Nonlinear population codes. Neural computation 16, 1105-1136.

Smith, M.A., and Kohn, A. (2008). Spatial and temporal scales of neuronal correlation in primary visual cortex. Journal of Neuroscience 28, 12591-12603.

Smith, R.L. (1975). Axonal projections and connections of the principal sensory trigeminal nucleus in the monkey. Journal of Comparative Neurology 163, 347-375.

Sorensen, S.A., Bernard, A., Menon, V., Royall, J.J., Glattfelder, K.J., Desta, T., Hirokawa, K., Mortrud, M., Miller, J.A., and Zeng, H. (2015). Correlated gene expression and target specificity demonstrate excitatory projection neuron diversity. Cerebral cortex 25, 433-449.

Tanke, N., Borst, J.G.G., and Houweling, A.R. (2018). Single-cell stimulation in barrel cortex influences psychophysical detection performance. Journal of Neuroscience 38, 2057-2068.

Tolhurst, D.J., Movshon, J.A., and Dean, A.F. (1983). The statistical reliability of signals in single neurons in cat and monkey visual cortex. Vision research 23, 775-785.

Tremblay, S., Pieper, F., Sachs, A., and Martinez-Trujillo, J. (2015). Attentional filtering of visual information by neuronal ensembles in the primate lateral prefrontal cortex. Neuron 85, 202-215.

Valente, M., Pica, G., Bondanelli, G., Moroni, M., Runyan, C.A., Morcos, A.S., Harvey, C.D., and Panzeri, S. (2021). Correlations enhance the behavioral readout of neural population activity in association cortex. Nature neuroscience 24, 975-986.

Van der Loos, H., and Woolsey, T.A. (1973). Somatosensory cortex: structural alterations following early injury to sense organs. Science 179, 395-398.

Veinante, P., and Deschênes, M. (1999). Single-and multi-whisker channels in the ascending projections from the principal trigeminal nucleus in the rat. Journal of Neuroscience 19, 5085-5095.

Wang, Q., Sporns, O., and Burkhalter, A. (2012). Network analysis of corticocortical connections reveals ventral and dorsal processing streams in mouse visual cortex. Journal of Neuroscience 32, 4386-4399.

Werner, G., and Mountcastle, V.B. (1963). The variability of central neural activity in a sensory system, and its implications for the central reflection of sensory events. Journal of Neurophysiology 26, 958-977.

Wilmes, K.A., and Clopath, C. (2019). Inhibitory microcircuits for top-down plasticity of sensory representations. Nature communications 10, 5055.

Woloszyn, L., and Sheinberg, D.L. (2012). Effects of long-term visual experience on responses of distinct classes of single units in inferior temporal cortex. Neuron 74, 193-205.

Woo, S.-H., Ranade, S., Weyer, A.D., Dubin, A.E., Baba, Y., Qiu, Z., Petrus, M., Miyamoto, T., Reddy, K., and Lumpkin, E.A. (2014). Piezo2 is required for Merkel-cell mechanotransduction. Nature 509, 622-626.

Woolsey, T.A., and Van der Loos, H. (1970). The structural organization of layer IV in the somatosensory region (SI) of mouse cerebral cortex: the description of a cortical field composed of discrete cytoarchitectonic units. Brain research 17, 205-242.

Xin, Y., Zhong, L., Zhang, Y., Zhou, T., Pan, J., and Xu, N.-l. (2019). Sensory-to-category transformation via dynamic reorganization of ensemble structures in mouse auditory cortex. Neuron 103, 909-921. e906.

Yamashita, T., Pala, A., Pedrido, L., Kremer, Y., Welker, E., and Petersen, C.C. (2013). Membrane potential dynamics of neocortical projection neurons driving target-specific signals. Neuron 80, 1477-1490.

Yamashita, T., and Petersen, C.C. (2016). Target-specific membrane potential dynamics of neocortical projection neurons during goal-directed behavior. elife 5, e15798.

Yang, T., and Maunsell, J.H. (2004). The effect of perceptual learning on neuronal responses in monkey visual area V4. Journal of Neuroscience 24, 1617-1626.

Yeganeh, F., Knauer, B., Guimarães Backhaus, R., Yang, J.-W., Stroh, A., Luhmann, H.J., and Stüttgen, M.C. (2022). Effects of optogenetic inhibition of a small fraction of parvalbumin-positive interneurons on the representation of sensory stimuli in mouse barrel cortex. Scientific Reports 12, 19419.

Zandvakili, A., and Kohn, A. (2015). Coordinated neuronal activity enhances corticocortical communication. Neuron 87, 827-839.

Zohary, E., Shadlen, M.N., and Newsome, W.T. (1994). Correlated neuronal discharge rate and its implications for psychophysical performance. Nature 370, 140-143.

Zucker, E., and Welker, W. (1969). Coding of somatic sensory input by vibrissae neurons in the rat's trigeminal ganglion. Brain research 12, 138-156.

Zylberberg, J., Pouget, A., Latham, P.E., and Shea-Brown, E. (2017). Robust information propagation through noisy neural circuits. PLoS computational biology 13, e1005497.

Chapter 2 Main Research

2.1 Approach

2.1.1 Mice

All procedures were in accordance with protocols approved by the University of Michigan Animal Care and Use Committee. We report calcium imaging experiments from 10 C57BL/J6 (Jackson Labs) mice from a C57BL/J6 background, with ages greater than 5 weeks (SI Appendix). Both sexes were used. Mice were housed in a vivarium with a reverse light-dark cycle (12 h each phase). Experiments occurred during the dark phase. After recovery from surgery (see below), mice were singly housed and water-restricted by giving them 1 mL per day. Mouse weight did not go below 70% of the starting weight. Procedures for surgery, virus injection, behavioral and calcium imaging experiments are described in detail in SI Appendix.

2.1.2 Surgery and Virus Injection

Mice were anesthetized with 1% isoflurane throughout surgery and kept on a thermal blanket to maintain body temperature. The scalp and periosteum over the skull were carefully removed. A circular craniotomy was made on the left hemisphere (3.0 mm diameter) with the dura left intact. The center of the craniotomy was located over the wS1 wS1 (3.5 mm lateral and 1.3 mm caudal relative to Bregma). Injections were performed unilaterally using a beveled glass pipette (30-50 μm diameter) mounted on an oil-based hydraulic micromanipulator (Narishige). Adeno-associated virus for

expressing GcaMP7f or 8f under the synapsin-1 promoter (AAV1-syn-jGCaMP7f-WPRE; Addgene 104488; AAV1-syn-jGCaMP7f-WPRE, Addgene 162376) was injected into the wS1 at depths of 250 µm and 120 µm below the dura and at a rate of 1 nL/sec (50 nL total per location). Injection was made at 3 different locations on the cortical surface around the coordinates given above. The craniotomy was covered with a glass window after the injection. The window was made by gluing two pieces of coverslip glass together. The smaller piece (3.0 mm diameter) was placed into the craniotomy and while the larger piece (4.0 mm diameter) was glued to the bone surrounding the craniotomy. Cyanoacrylate adhesive (KrazyGlue) and dental acrylic (Jet Repair Acrylic) were used to secure a titanium head post in place on the skull. Silicone elastomer (Kwik-Cast, WPI) was placed over the window for protection during the recovery period. The mouse was allowed to recover for at least 10 days before moving to water restriction. Imaging started 3-5 weeks after surgery.

2.1.3 Behavioral Task – Discrimination Task

Head-restrained mice were trained to perform a frequency discrimination task using a behavioral apparatus controlled by BPod (Sanworks). Mice were placed in an acrylic (4.5 cm inner diameter) tube. For 7–10 d before training, mice received 1 ml per day of water. Mice were weighed prior to and after training sessions to ensure the amount of water consumed. In the first 3 sessions (‘Habituation’), mice were allowed to freely lick at the water port positioned near its snout. Each time the tongue crossed the infrared beam to touch the water port, the mouse received a drop of water (~7 µL). In the next 2 sessions (‘Go only’), mice were conditioned to lick at the water port to a passive whisker deflection. Facial whiskers were threaded through a plastic mesh

attached to a piezoelectric actuator (CTS). For training in ‘Go/NoGo’ sessions (2-4 days), the whiskers were deflected for 1 s with sinusoidal deflection (rostral to caudal) at 30 Hz (Go trials) or 5 Hz (NoGo trials). Go and NoGo trials each comprised 50% of all trials, therefore stimulus categories were equally represented in the data. 0.1-s auditory tone (8 kHz, ~70 dB SPL) was delivered starting 2 s before whisker stimulus onset, followed by a 0.5-s ‘No-lick’ window. If mice lick during this window, the trial was defined as ‘Premature Licking’ and aborted. Licks occurring during the first 1.2 sec after the onset of whisker deflection had no consequence. The ‘reward window’ was defined as 1.2 – 3.2 s after the onset of whisker deflection. The Go trials resulted in a ‘hit’ when the mouse licked the water port within the reward window and received a drop of water. A ‘miss’ occurred if mice did not lick within the reward window, and no reward or punishment was delivered. The NoGo trials resulted in a ‘false alarm’ if mice had licked within the reward window, and mice were punished by a 5.00 s time-out. Licking during time-out resulted in an additional time-out. A ‘correct rejection’ occurred if mice did not lick within the reward window on NoGo trials. In the next 2-4 sessions (‘Self-initiated Go/NoGo’), mice were trained to initiate each Go or NoGo trial by turning a wheel (Lego) attached to a rotary encoder more than 65 degree in either direction. The task itself was otherwise identical to the previous stage. At the last phase (‘discrimination task’), the whiskers were stimulated for 1 s at a varied frequency. In ‘High-Go’ paradigm, whiskers were deflected for 1 s at a frequency randomly selected from 20, 25, 30, 40, 50 Hz on ‘Go’ trials and 2, 5, 10, 15 Hz on ‘NoGo’ trials. In ‘Low-Go’ version of the task, the contingency was reversed. During all sessions, ambient white noise (cut off at 40 kHz, ~60 dB SPL) was played through a separate speaker to mask any other

potential auditory cues associated with movement of the piezoelectric actuator. No more than 3 trials of the same type occurred in a row. The fraction of correct trials (Fraction Correct/FC) was defined as the number of hits plus correct rejections divided by the total number of Go and NoGo trials. The hit rate was defined as the number of hits divided by the total number of Go trials. The false alarm rate was defined as the number of false alarms divided by the total number of NoGo trials. Mice were considered trained once the performance was > 70 % correct. d-prime was calculated as z(hit rate) - z(false alarm rate). Mice reached this performance criteria after 10 -12 daily training sessions.

2.1.4 wS1 Lesion and Silencing Experiments

After confirming that mice reached >70% performance in the frequency discrimination task, we inactivated wS1 by either aspirating the cortical tissue with gentle vacuum suction or stereotaxically injecting GABAa receptor agonist muscimol in the wS1 (3.5 mm lateral and 1.3 mm caudal relative to Bregma) under anesthesia with 1% isoflurane. For silencing with muscimol (5 mg / ml), injections occurred at three different depths (200, 400, 600 µm; 50 nl each) from the pial surface. The craniotomy was sealed with silicone sealant (KwikCast) following injection and covered with a thin layer of dental cement. Behavioral performance in the frequency discrimination task was monitored after recovery from anesthesia (1 h). In the following day, we tested the effect of saline injected into wS1 on behavior using the same method as outlined above.

2.1.5 Two-Photon Calcium Imaging of Layer 2/3 Somata

Images were acquired on a Scientifica two-photon microscope (Hyperscope) equipped with an 8 kHz resonant scanning module, 2 GaAsP photomultiplier tube

modules, and a 16× 0.8 NA microscope objective (Nikon). GCaMP was excited at 960 nm (40-60 mW at specimen) with an InSight X3 tunable ultrafast Ti:Sapphire laser (Spectra-Physics, Santa Clara, CA, USA). Imaging fields were restricted to areas where GCaMP expression overlapped with the center of the cranial window (3.5 mm lateral and 1.3 mm caudal to Bregma). The beam was focused to 150 – 250 µm from the cortical surface. The field of view ranged from 458 µm x 344 µm to 275 µm x 207 µm. Images were acquired with a resolution of 512 x 512 pixels at 30 Hz using ScanImage. A movie for a single trial consisted of 200 frames.

2.1.6 Image Analysis

Image stacks were processed using Suite2P pipeline (38). Procedures for ROC analysis, neuronal correlation calculations and population decoding analysis are described in SI Appendix. After correcting for motion, regions of interest (ROIs) were selected and then manually curated to remove ROIs that were not neurons. The neuropil fluorescence time series was multiplied with a correction factor of 0.7 and then subtracted from the raw fluorescence time series to obtain the corrected fluorescence time series: Fcorrected(t) = Fraw - Fneuropil * 0.7. ΔF/Fo was calculated as (F- Fo) / Fo, where Fo represents the baseline fluorescence calculated by determining the average fluorescence (F) during 500-167 ms time window preceding whisker stimulus onset. Evoked ΔF/Fo responses were calculated as the average ΔF/Fo over 21 frames following the onset of whisker stimulus delivery minus the average ΔF/Fo over the 5-15th frames preceding the onset of whisker stimulus delivery. To assign each neuron as 'responsive' or 'non-responsive', the averaged standard deviation of baseline ΔF/Fo for each neuron was calculated. For each neuron each trial, if there are at least 3 frames

during the 21 frames after onset of stimulus have ΔF/Fo three standard deviations greater than Fo, the neuron was considered responsive at that trial. Neurons that were responsive in more than 8% of the trials during the session were considered responsive neurons.

2.1.7 Single neuron ROC Analysis

The receiver operating characteristic (ROC) analysis was used to calculate the 'stimulus probability'. A decision variable (DV) was assigned for each trial based on the response of the particular neuron. DV was the evoked ΔF/Fo as defined above. Trials were grouped by the stimulus category (High vs. Low) and for each behavioral state for stimulus probability and an ROC curve was obtained by systematically varying the criterion value across the full range of DV using the MATLAB 'perfcurve' function. The area under the ROC curve (AUC) represents performance for an ideal observer in categorizing trials based on the DV. Stimulus probability (SP) was the AUC for discriminating the stimulus condition.

2.1.8 Noise and Signal Correlation Analyses

We calculated across-neuron pairwise noise correlations between neuron pairs recorded at the same time in a single session, across trials sharing the same stimulus frequency (16). Evoked ΔF/Fo responses for each neuron were z-scored within each stimulus frequency. Noise correlation was then calculated as the Pearson correlation coefficient of the z-scored responses of two neurons across trials. We calculated pairwise signal correlations as the similarity of frequency tuning between neuron pairs recorded at the same time in a single session. Average evoked ΔF/Fo responses were

calculated for each stimulus frequency and z-scored across all stimulus frequencies for each neuron. The stimulus frequency associated with maximal z-score was defined as the preferred frequency for each neuron. Signal correlation was calculated as the Pearson correlation coefficient of the z-scored responses of two neurons across stimulus frequencies. To cancel out the effect of noise correlation without impacting the tuning property of individual neurons, trial labels were shuffled 100 times within each stimulating frequency for each neuron.

2.1.9 Population Decoding

The Support Vector Machine (SVM, Python sklearn package) with linear kernel was used to decode the stimulus categories or behavioral choices from the vector of z-scored evoked ΔF/Fo responses. For each session, the SVM classifier was trained using labels for stimulus (1 for 'Go', 0 for "Nogo') or behavioral choices (1 for 'Licking', 0 for 'Nolick') and tested with a nested 5-fold cross-validation scheme. 80% of the trials were randomly selected for training and the remaining 20% of the trials were used for testing. Classifier performance was evaluated as label-prediction accuracy. The final prediction accuracy was generated from 100 times of repeating training and testing classifier. All classifiers were regularized using L2-regularization. The regularization parameter was optimized through a pre-training session where the best penalty parameter that yields the highest accuracy was chosen. According to design of the behavioral paradigm, each session had well-balanced number of trials of two stimulus categories but may have unbalanced choices. To avoid the effect of unbalanced numbers of trials, subsets of 'Lick' trials or 'No-lick' trials were randomly subsampled to match the number of trials across different trial types.

2.1.10 Statistics

Error bars indicate mean ± SEM unless mentioned otherwise. All statistical tests are two-tailed.

2.2 Results

2.2.1 Mice Learn to Discriminate Whisker Vibration Frequencies Using wS1

We trained head-fixed mice to perform a vibration frequency discrimination task in which they report, by licking or withholding licking, whether whiskers received a high- or low-frequency sinusoidal deflection (Figure 6A). Mice initiated each trial by manually turning a wheel, which was followed by a brief auditory tone (8 kHz, 0.1 s, ~70 dB SPL) indicating the beginning of a trial. Facial whiskers were threaded into a mesh attached to a piezoelectric bender and deflected for 1 s at a frequency randomly selected from 20, 25, 30, 40, 50 Hz on 'Go' trials (50% of all trials). On 'NoGo' trials (50% of all trials), whiskers were deflected at a frequency selected from 2, 5, 10, 15 Hz. A response window where Go cued licking was rewarded began after a 1.2-s delay following the onset of whisker deflection. Licking during the delay period had no behavioral consequences. Licking to the NoGo cue during the response window resulted in a brief (3 s) time-out. Trial outcomes comprised a mixture of successful responses ("Hits") and failed responses ("Misses") following Go stimulus delivery, as well as correct omission of licking ("Correct Rejection") and incorrect ("False Alarms") licking responses in the presence of the NoGo stimulus. Premature licking during the 'No-lick window', which lasted for 0.5 s after the trial initiation, led to a trial abortion.

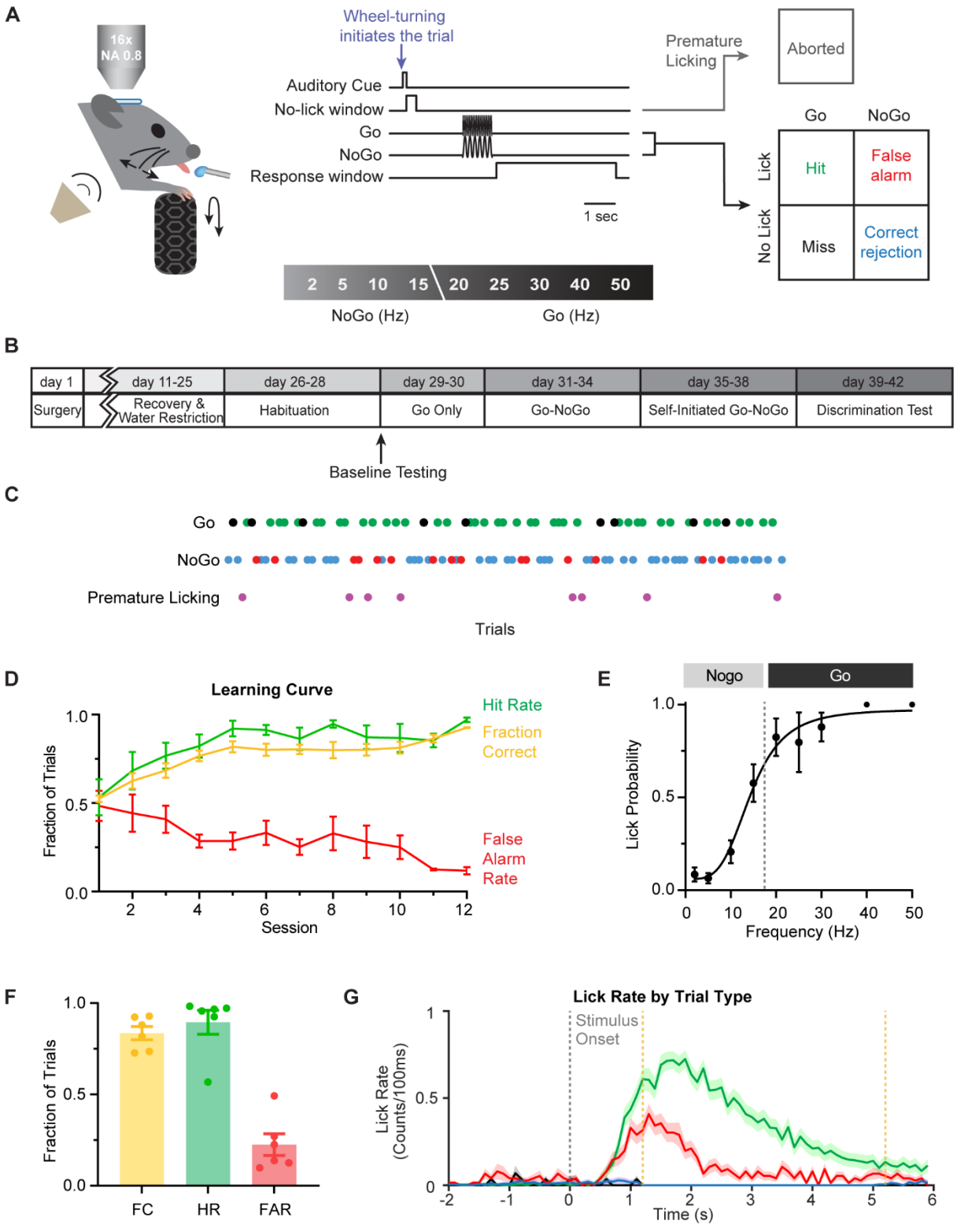

Figure 6. Whisker vibration frequency discrimination task in head-fixed mice. (A) Schematic showing behavior set-up and task structure. Water-restricted mice were trained to initiate each trial and lick the

water port if the frequency of whisker vibration by a piezoelectric stimulator is 'high' (20, 25, 30, 40 or 50 Hz; Go cue) and withhold licking if it is 'low' (2, 5, 10 or 15 Hz; NoGo cue). Go and NoGo trials each comprised 50% of all trials. A 0.1-s auditory tone (8 kHz, ~70 dB SPL) was delivered starting 2 s before whisker stimulus onset, followed by a 0.5-s 'No-lick' window. If mice licked during this window, the trial was defined as 'Premature Licking' and aborted. Licks occurring during the first 1.2 sec after whisker stimulus onset had no consequence. The 'reward window' was defined as 1.2 – 5.2 s after the whisker stimulus onset. (B) Experimental timeline. (C) Representative session showing trials with hit (green), miss (black), false alarm (red), correct rejection (blue) and premature licking (purple). (D) Behavioral performance averaged across late lickers trained under 'High-Go' paradigm as a function of training sessions (n = 6 mice). (E) Average psychometric function of all animals trained under 'High-Go' paradigm (n = 6 mice). The dashed black line marks the experimentally defined Go/NoGo category boundary. (F) Average fraction of correct trials (FC), hit rate (HR) and false alarm rate (FAR) of expert mice (n = 6 mice). FC: 0.836 ± 0.037; HR: 0.896 ± 0.066; FAR: 0.225 ± 0.060. (G) Distribution of licks in 100 ms bins within trials with hit (green), miss (black), false alarm (red), correct rejection (blue). The dashed gray line indicates the onset of whisker deflection. The dashed yellow lines mark the onset and offset of the reward window.

Mice were trained in multiple phases (Figure 6B). After habituation to head-fixation, they performed the 'Go Only' task which included trials with 30 Hz whisker vibration only. Licking during the response window was rewarded. During the 'Go / NoGo' phase, mice were trained to discriminate between 30 Hz ('Go') and 5 Hz ('NoGo') stimuli. When the fraction of correct trials reached 80%, the task was switched to 'Self-initiated Go / NoGo' phase where they learned to initiate each trial by manually turning a wheel. Finally, in the 'Discrimination Test' phase, the full range of vibration frequencies were introduced. Mice typically completed 120-150 trials per session (Figure 6C). A separate group of mice was subjected to a 'Passive Exposure' condition. These mice were water-restricted and went through the same number of sessions as the experimental group except that licking had no behavioral consequences under this condition. They were allowed to drink water freely from the lick-port after each training session ended.

The fraction of correct trials increased throughout training, mainly due to a gradual decrease in the fraction of incorrect responses on NoGo trials (i.e. FAR) (Figure 6D). It typically took 10-12 daily training sessions for mice to become an 'expert' at the

discrimination task, defined as the fraction of correct trials greater than 0.7. The performance curve of expert mice shows a sigmoid relationship between lick probability and stimulus frequency, indicating categorical decision making (Figure 6E). Expert mice licked preferentially in response to Go cues (fraction correct: 0.836 ± 0.037; hit rate: 0.896 ± 0.066; false alarm rate: 0.225 ± 0.060; n = 6 mice) (Figure 6F). Lack of response is somewhat difficult to interpret in a typical Go / NoGo task. The self-paced nature of this task resolves this issue to some extent; not licking reflects a correct behavioral response (on NoGo trials) or a perceptual error (on Go trials) rather than inattention or lack of motivation. After training, the number of licks on Go trials did not peak immediately, but with a delay of ~1.5 s after the stimulus onset, probably due to the 1.2 s delay before the beginning of response window. Mice consistently withheld licking during the first 0.70 s of the 1.2 s delay period (Figure 6G).

Before characterizing learning-induced modifications in wS1, we tested if contralateral wS1 contributes to the tactile frequency discrimination. The ipsilateral wS1 was known to show weak and non-differentiable responses to whisker stimulations to the same side of the face. Hence, it wasn't the target of this study. We inactivated wS1 by aspirating the contralateral cortical tissue in wS1 area (N = 3 mice) (Figure 7A). The slope of the performance curve after contralateral wS1 ablation decreased in all mice, compared with pre-lesion performance (Figures 7B and 7C). Performance curves of individual mice reflected the same trend (Figures 7D). This result is consistent with previous studies showing that acute inactivation of the wS1 impairs task performance (Hong et al., 2018; Miyashita and Feldman, 2013). Licking on NoGo cues, including in response to 5 Hz stimuli, increased with wS1 inactivation but returned to baseline level

with additional training, consistent with previous studies (Figure 7E) (Hong et al., 2018; Hutson and Masterton, 1986). These results demonstrate that wS1 is critical for efficient tactile frequency discrimination.

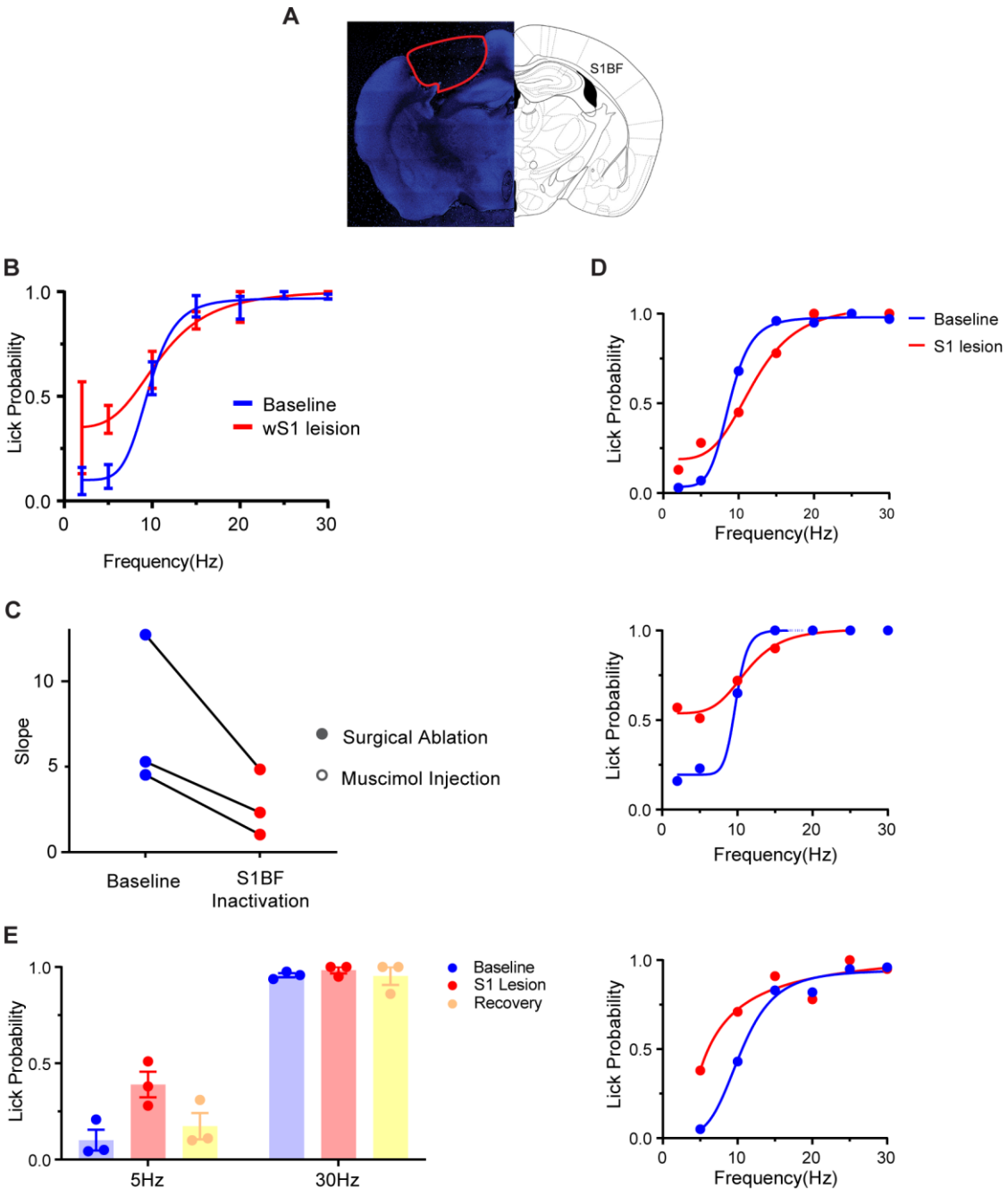

Figure 7.Efficient tactile frequency discrimination requires intact wS1. (A) wS1 containing barrel field (BF) was carefully removed in animals trained to perform the frequency discrimination task. Red line outlines the cortical tissue that was removed. (B) Psychometric curves that depict the probability with which the

stimulus was perceived 'high' in relation to stimulus frequency, before versus after the wS1 inactivation. (C) The slope of psychometric function was reduced in all tested animals (n = 3 mice). (D) Performance curves of well-trained individual mice at baseline (blue) and 1 day post wS1 removal (red).. (E) Average lick probability on 5 Hz and 30 Hz trials at baseline (blue), 1 day (red) and 4 days (yellow) post wS1 removal (n = 3 mice).

2.2.2 Learning Enhances Category Representation among L2/3 Neurons of wS1

To determine the neural correlates of learning, we monitored stimulus-evoked responses of L2/3 neurons using *in vivo* two-photon imaging of the genetically encoded calcium indicator GCaMP7f or 8f (Figure 8A) (Dana et al., 2019). We compared the frequency selectivity of individual neurons in response to whisker vibration at nine different frequencies randomly delivered during task performance before and after mice learned the task. Our analysis was based on comparisons of the same imaging field, and the same subpopulation of neurons, before versus after learning (Figure 8B), although responses from individual neurons were not compared across training sessions. To characterize frequency tuning of individual neurons, mean stimulus-evoked $\Delta F/F_0$ responses were calculated using frames within 0.7 s (21 frames) after whisker stimulus onset, and they were z-scored across all frequencies. This time window was used in all subsequent analyses to avoid potential confounding effects related to licking (Figure 6G). The stimulus frequency that elicited maximal z-scored $\Delta F/F_0$ in a given neuron was defined as its 'preferred frequency'. We pooled neuronal tuning curves (i.e., z-scored $\Delta F/F_0$ across nine different frequencies) across mice and sorted them by their preferred frequency. All tested vibration frequencies were represented by L2/3 neurons in wS1 of naive mice (Figures 8C and 8D). Importantly, training in the frequency discrimination task resulted in broadening of neuronal tuning curves within Go and NoGo stimulus categories (Figure 8C), whereas passive exposure had little effect on tuning curves (Figure 8D). We averaged the nine $\Delta F/F_0$ z-scores (i.e.

individual tuning curves) across subpopulations of neurons that share the same preferred frequency. Learning resulted in broadening of subpopulation tuning curves at most frequencies within each category (NoGo: 2, 5 and 10 Hz; Go: 30, 40 and 50 Hz), whereas they remained relatively unchanged at categorical boundary frequencies (15 Hz and 20 Hz) (Figure 8E). We also compared the frequency tuning curves before versus after passive exposure in a separate group of mice. Little change in tuning curves was observed under this passive exposure condition (Figure 8F).

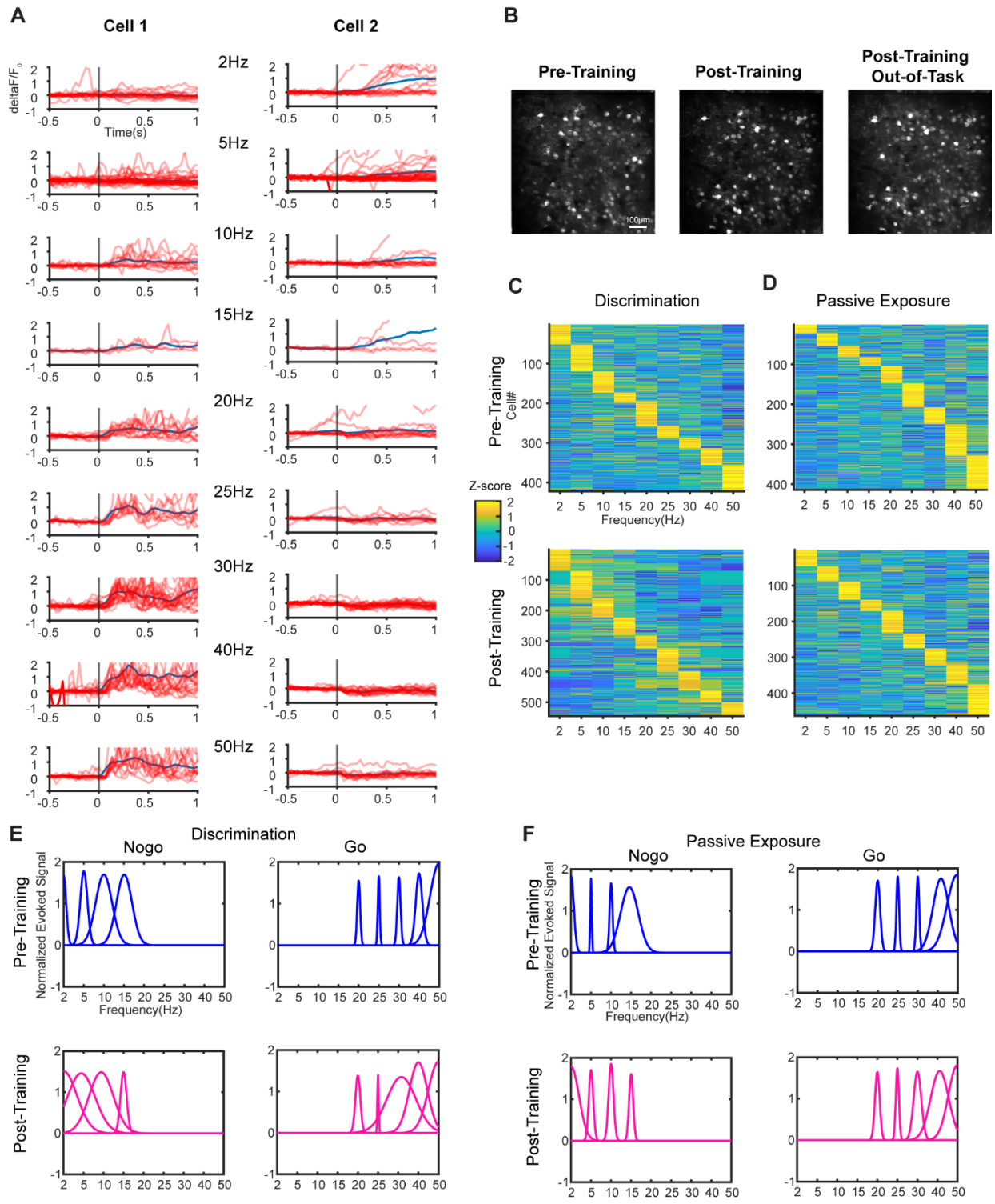

Figure 8. Training in tactile discrimination alters neuronal tuning in L2/3 of wS1. (A) Representative examples of GCaMP7f-expressing cells in L2/3 of wS1 that respond to either Go cues (Cell 1) or NoGo cues (Cell 2). The two cells were present in the same field of view, and their activities recorded in the same session. Red and blue traces indicate raw ΔF/Fo over time from individual trials and their average, respectively. (B) Example field of view showing GCaMP7f-expressing neurons, generated by calculating maximum fluorescence across z-axis of image stacks from 10 randomly selected trials of a pre-training

session, post-training session, and post-training out-of-task session. (C) Frequency tuning of individual neurons, before (top) and after (bottom) training in the discrimination task. Color bar indicates z-score of mean evoked ΔF/F0 response, calculated using frames within the first 700 ms after stimulus onset. Neurons in the heatmaps are sorted by 'preferred frequency' - i.e., the stimulus frequency associated with peak evoked ΔF/F0 - in the ascending order. Heatmaps were calculated using baseline testing sessions and sessions after the animals became an expert at the frequency discrimination. (D) Same as C but for the control group (Passive exposure) that underwent the same procedure as trained mice except that licking did not result in reward or punishment in this group. (E) Frequency tuning of L2/3 population estimated using Gaussian function fitted to the average tuning curve derived from neurons with the same preferred frequency. Mean stimulus-evoked signals were z-scored across all frequencies to generate single neuron tuning curves. (F) Same as E but for the passive exposure control.

To gain insight into learning-induced changes in the category selectivity of individual neurons, we quantified the response selectivity for Go versus NoGo category using ROC analysis. 'Stimulus Probability' captures how well an ideal observer could categorize a sensory stimulus (in our case, high vs. low-frequency vibration) based on the neural response in a trial-by-trial manner with 0.5 indicating lack of selectivity towards either category (Kwon et al., 2016). We used stimulus-evoked $\Delta F/F_o$ as a decision variable for individual trials. Training in the discrimination task pushed the distribution of stimulus probability towards the two extremes (median [Interquartile range / IQR] for pre-training: 0.495 [0.098]; post-training: 0.459 [0.331]). Comparing to the passive exposure group (0% → 0% SP < 0.25, 0% → 1.45% SP>0.75), the discrimination group shows a massive increase in cells below 0.25 and above 0.75 in post-training (0.52% → 15.39% SP < 0.25, 0.74%→ 12.79% SP>0.75). This indicates an increase in the number of neurons representing either stimulus category (Figure 9A). Passive exposure to repeated whisker stimulation also slightly increased the width of stimulus probability distribution (Figure 9B), but the effect was subtle compared with active discrimination learning (median [IQR] for pre-training: 0.528 [0.081]; post-training: 0.508 [0.133]). Therefore, tactile discrimination learning enhances encoding of stimulus category by individual L2/3 neurons of wS1, whereas passive exposure to a repeated tactile stimulation does not. Our results extend growing evidence supporting that

perceptual learning is accompanied by enhanced representation of task-relevant features in primary sensory cortex (Corbo et al., 2022; Kato et al., 2015; Poort et al., 2015; Schoups et al., 2001; Schumacher et al., 2022; Xin et al., 2019).

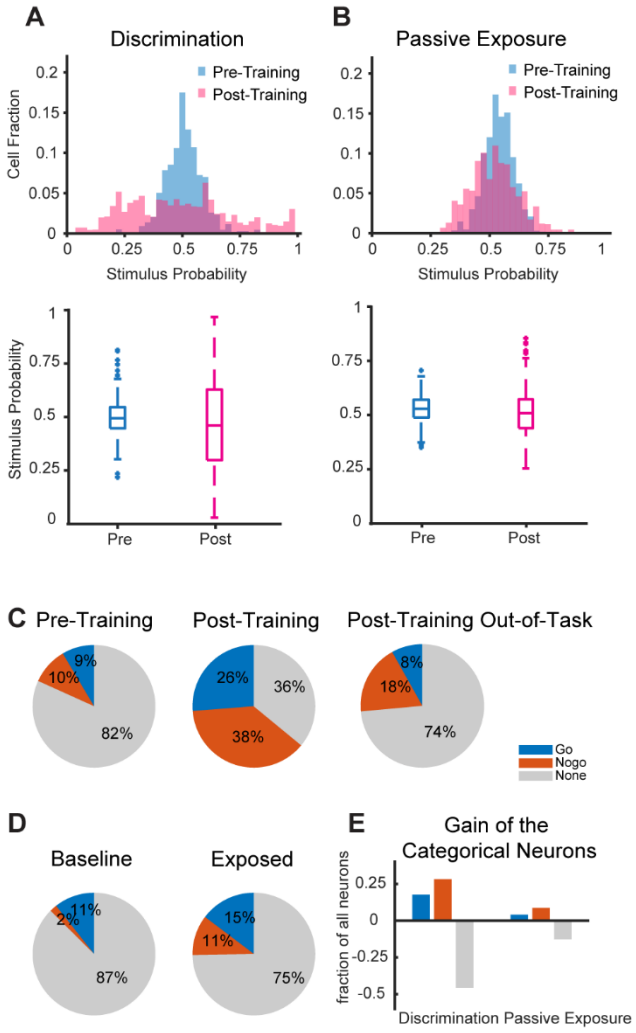

Figure 9. Training in tactile discrimination increases category selectivity of L2/3 neurons in wS1. (A) (top) Histograms showing stimulus probability, a ROC-based metric that quantifies trial-by-trial co-fluctuation of neuronal response (evoked ΔF/F0) and stimulus category (Go or NoGo). (bottom) Box and whisker plots showing median and interquartile range of stimulus probability values from pre- (blue) and post-training (magenta) sessions. Pre-Training: Median SP = 0.495, 25 percentile SP = 0.447, 75 percentile SP = 0.545, Interquartile Range (IQR) = 0.098. Post-Training: Median SP = 0.459, 25 percentile SP = 0.296, 75 percentile SP = 0.627, IQR = 0.331. (B) Same as A but for the passive exposure control. Pre-Exposure: Median SP = 0.528, 25 percentile SP = 0.488, 75 percentile SP = 0.569, IQR = 0.081. Post-Exposure: Median SP = 0.508, 25 percentile SP = 0.439, 75 percentile SP = 0.572, IQR = 0.133. (C) (Left) Pie chart of proportions of 'Go' category neurons (blue), 'NoGo' category neurons (orange), and non-categorical neurons (grey) in pre-training sessions (n = 6 mice). Cells with 95% CI of stimulus probability (SP) > 0.5 are defined as 'Go' category neurons, < 0.5 as 'NoGo' category neurons. If 95% CI of SP includes 0.5, they were defined as non-categorical. (Middle) same as left but for post-training sessions (n = 6 mice). (Right) same as left but for post-training out-of-task sessions (n = 4 mice). (D) (Left) same as C left but for

the passive exposure group during baseline sessions (n = 4 mice). (Right) same as C left but for post-passive exposure sessions (n = 4 mice). (E) Change in fractions of 'Go', 'NoGo', and non-categorical neurons through discrimination training or passive exposure to repeated stimulation.

2.2.3 Enhanced Category Selectivity in wS1 Neurons is Context-Dependent

An unanswered question is whether this enhancement of category encoding in wS1 neurons is only evident during discrimination task performance or persists outside the behavioral paradigm. If the enhanced category selectivity is primarily driven by local synaptic plasticity, it should extend to stimuli presented outside of the task performance. On the other hand, context-dependent enhancement of category selectivity would point to top-down modulation playing a role in the expression of learning-induced changes. To address these issues, we examined the presence of training-induced category selectivity in trained mice behaviorally disengaged from the task. We characterized frequency tuning of L2/3 neurons in a subset of well-trained mice that were satiated for water (4 mice) following the task performance on the same day. We found that the distribution of the peak of activity became comparable to that observed in pre-training sessions (Figure 10A). Learning-induced broadening of neuronal tuning curves was not evident at any stimulus frequency (Figure 10B). The distribution of stimulus probability was also comparable to that found in naive animals (Figures 10C and 10D). Therefore, the learning-induced enhancement in encoding of stimulus category is expressed specifically during task performance.

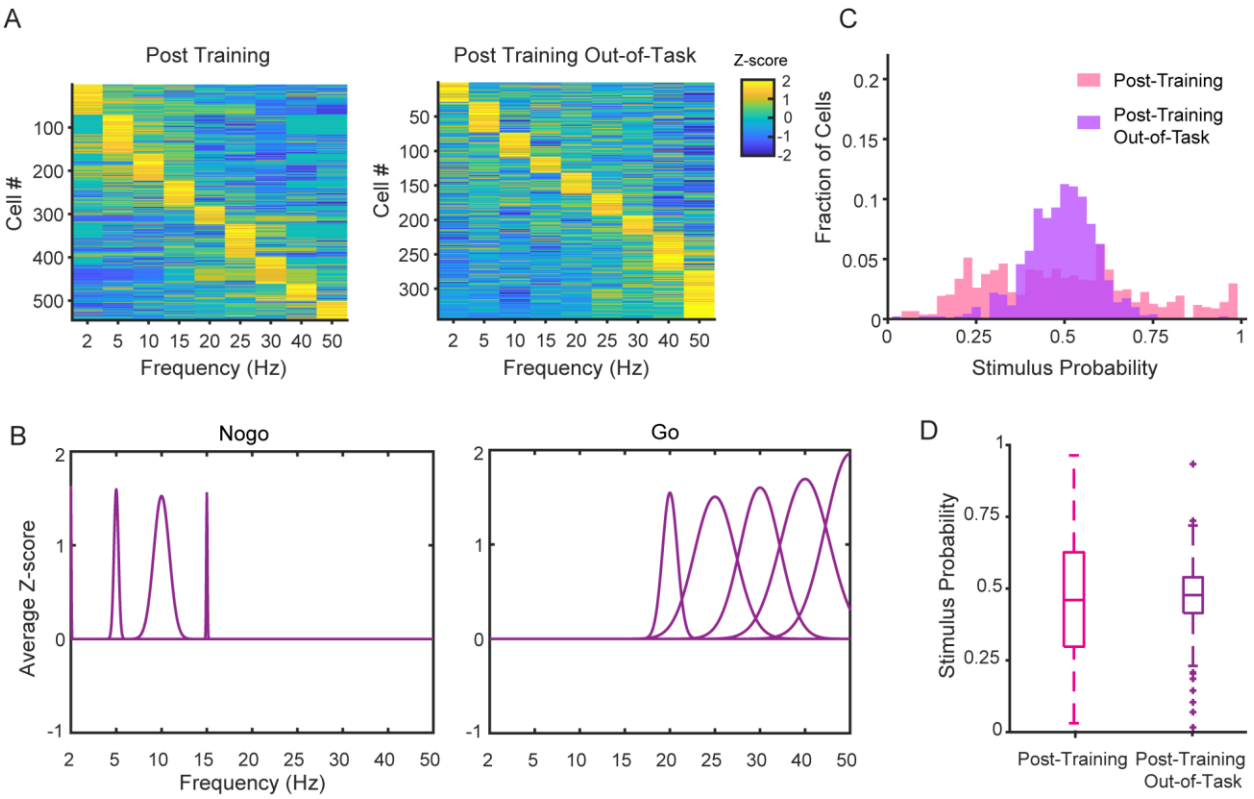

Figure 10. Enhanced category representations are context-dependent. (A) Frequency tuning of individual wS1 L2/3 neurons from post-learning sessions during task performance versus out-of-task. (B) Frequency tuning of L2/3 population. Mean stimulus-evoked signals were z-scored across all frequencies to generate a tuning curve for each neuron. Population tuning curves were then estimated using Gaussian function fitted to the average tuning curve calculated from neurons that share the same preferred frequency. (C) Histogram showing distribution of stimulus probability of individual neurons from post-training in-task (data from Figure 5F) and out-of-task conditions. (D) Box and whisker plot showing stimulus probability of individual neurons from post training in-task (data from Figure 5F) and out-of-task conditions. Out-of-task: median SP = 0.481, 25 percentile SP = 0.419, 75 percentile SP = 0.543, IQR = 0.124.

2.2.4 Learning Increases Correlations Among Neurons Based on Their Stimulus Category in a Context-Dependent Manner

Analyses described thus far focused on the frequency tuning of individual wS1 neurons. Prior studies have demonstrated that perceptual learning can primarily alter noise correlations, relationships of signal and noise correlations, and/or population coding even when there is little effect on neuronal tuning (Gu et al., 2011; Jeanne et al., 2013; Ni et al., 2018). We next tested whether increases in category selectivity of individual neurons are accompanied by network-level reorganization by focusing on

neuronal correlations in wS1. Pairwise signal and noise correlations respectively quantify tuning curve similarity and trial-to-trial co-variability of responses (Cohen and Kohn, 2011). Noise correlations are an estimate of synaptic connectivity and/or shared inputs (Ko et al., 2011). By recording large cell populations over a broad range of stimulus frequencies, we were able to estimate 'correlation matrices' – i.e., how signal and noise correlations vary as a function of combinations of frequency preferences in cell pairs. We observed learning-induced enhancement of signal correlations (or frequency tuning similarity) among cell pairs that shared a preferred category. Learning increased signal correlations among pairs that shared a preference toward Go cues (high frequency, Figures 11A and 11B) (pre: 0.100 ± 0.006, post: 0.354 ± 0.007), possibly by selectively broadening their tuning toward multiple frequencies associated with reward (Figure 10D). Likewise, signal correlations among cell pairs that prefer NoGo cues (low frequency) significantly increased through learning (pre: 0.209 ± 0.006, post: 0.461 ± 0.005). Signal correlations across two pools of neurons that prefer opposite categories (Go-NoGo) became strongly negative (pre: -0.062 ± 0.004, post: -0.287 ± 0.004), suggesting they became more dissimilar (Figures 11A and 11B). Although passive exposure resulted in statistically significant changes in signal correlations, the magnitude of change was much smaller compared with what occurred during discrimination task learning. Moreover, Go-Go pairs showed a decrease, rather than an increase, of signal correlations under passive exposure (Figure 11C and 11D). Therefore, learning enhances tuning similarity in L2/3 neurons in a category-aligned

manner.

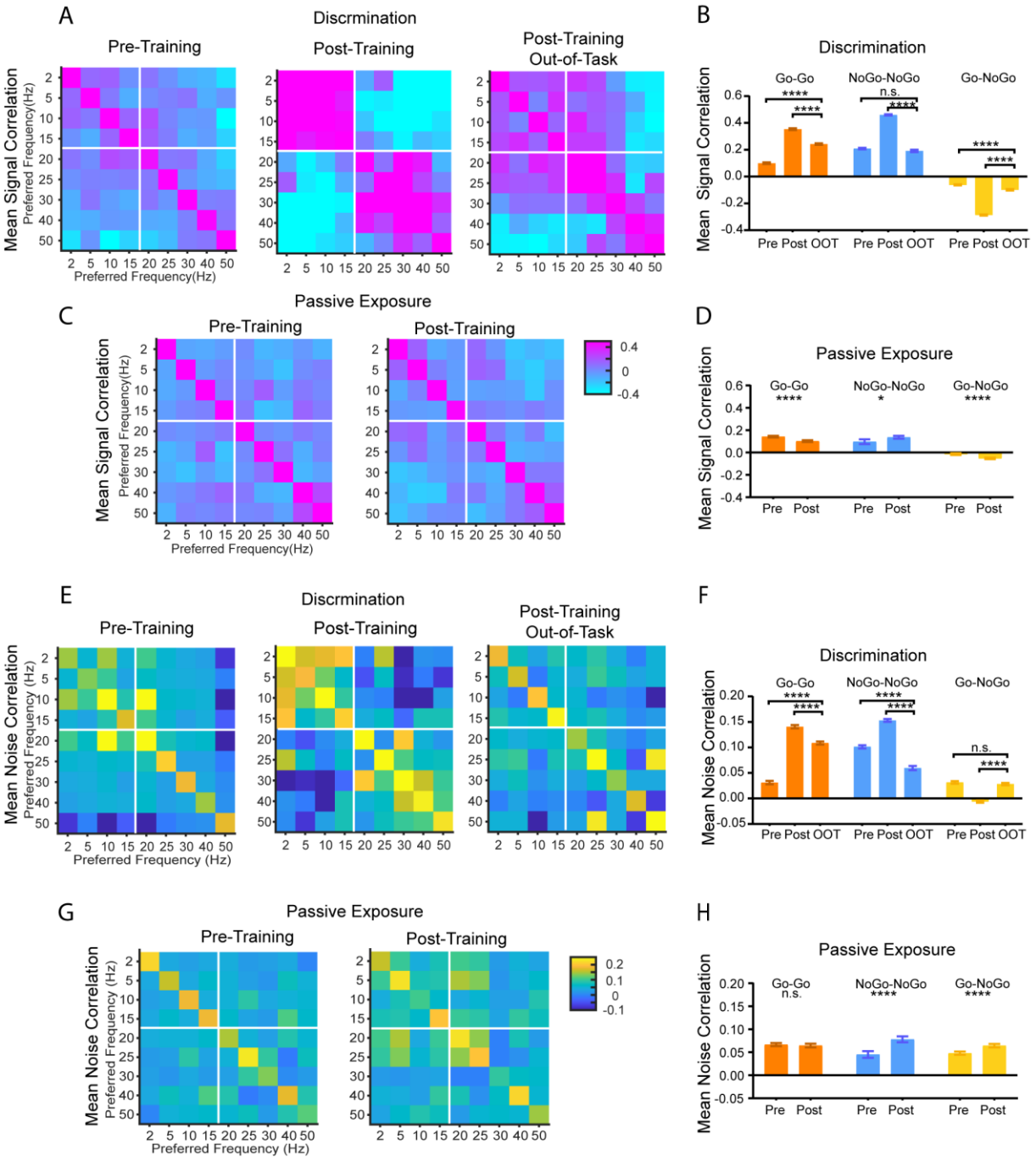

Figure 11. Neurons with shared category preference show an increase in correlations. (A) Color in each bin indicates mean pairwise signal correlation among neurons whose preferred frequency is indicated by x and y coordinate of that bin. Left, middle, and right panels represent data before, after discrimination training, and after training out of task status. White lines indicate the boundary between Go and NoGo cues. (B) Mean signal correlations in expert animals during out-of-task (OOT) sessions. OOT: Go-Go (orange), 0.242 ± 0.006; NoGo-NoGo (blue), 0.192 ± 0.009; Go-NoGo (yellow), -0.099 ± 0.005. Pre-training vs. OOT: t = 16.54, p < 0.0001, df = 11514; post-training vs. OOT: t = 12.67, p < 0.0001, df = 12545; pre-training vs. OOT: t = 1.686, p = 0.0918, df = 6280; post-training vs. OOT: t = 25.82, p <

0.0001, df = 9347; pre-training vs. OOT: t = 5.778, p < 0.0001, df = 15993; post-training vs. OOT: t = 26.78, p < 0.0001, df = 20127. Unpaired t-tests. (C) Same as (A) but for passive exposure group. (D) Mean signal correlations among pairs that share the same category preference ('Go-Go' or 'NoGo-NoGo' pairs) were prominently elevated in expert animals (Post) compared with novice (Pre). Go-Go (orange), pre: 0.100 ± 0.006, post: 0.354 ± 0.007, t=27.75, df = 11483, p < 0.0001; NoGo-NoGo (blue), pre: 0.209 ± 0.006, post: 0.461 ± 0.005, t=31.82, df = 11459, p < 0.0001. Mean signal correlations across neurons that prefer different categories ('Go-NoGo' pairs) showed significant decreases after learning. Go-NoGo (yellow), pre: -0.062 ± 0.004, post: -0.287 ± 0.004, t= 35.94, df = 22090, p < 0.0001 (unpaired t-test). Mean signal correlations either decreased or slightly increased among pairs that share the same category preference ('Go-Go' or 'NoGo-NoGo' pairs) after the passive exposure (post) compared with the baseline (pre). Go-Go (orange), pre: 0.142 ± 0.004, post: 0.102 ± 0.004, t=7.445, df = 24772, p < 0.0001; NoGo-NoGo (blue), pre: 0.097 ± 0.011, post: 0.136 ± 0.006, t = 3.091, df = 5329, p = 0.026. Mean signal correlations across neurons that prefer different categories (Go-NoGo) showed modest but significant decreases. Go-NoGo (yellow), pre: -0.014 ± 0.004, post: -0.053 ± 0.003, t = 7.391, df = 21743, p < 0.0001. Unpaired t-test for all comparisons. (E) Color in each bin indicates mean pairwise noise correlation among neurons whose preferred frequency is indicated by x and y coordinate of that bin. Left, middle, and right panels represent data before, after discrimination training, and after training out of task status. White lines indicate the boundary between Go and NoGo cues. (F) Mean noise correlations among pairs that share the same category preference ('Go-Go' or 'NoGo-NoGo' pairs) were higher in expert animals (post) compared with novice (pre). Go-Go (orange), pre: 0.031 ± 0.003, post: 0.141 ± 0.003, t=23.45, df = 11483, p < 0.0001; NoGo-NoGo (blue), pre: 0.101 ± 0.003, post: 0.153 ± 0.003, t=11.85, df = 11459, p < 0.0001; On the other hand, mean noise correlations decreased across neurons that prefer different categories (Go-NoGo) in expert animals. Go-NoGo (yellow), pre: 0.032 ± 0.002, post: -0.006 ± 0.002, t= 11.19, df = 22090, p < 0.0001. Unpaired t-test for all comparisons. OOT: Go-Go (orange), 0.109 ± 0.003; NoGo-NoGo (blue), 0.060 ± 0.004; Go-NoGo (yellow), 0.028 ± 0.002. Pre-training vs. OOT: t = 17.35, p < 0.0001, df = 11514; post-training vs. OOT: t = 7.194, p < 0.0001, df = 12545; pre-training vs. OOT: t = 7.722, p < 0.0001, df = 6280; post-training vs. OOT: t = 16.76, p < 0.0001, df = 9347; pre-training vs. OOT: t = 0.9408, p = 0.3468, df = 15993; post-training vs. OOT: t = 9.880, p < 0.0001, df = 20127. Unpaired t-tests. (G) Same as (E) but for passive exposure group. (H) Mean noise correlations did not change among pairs that prefer 'Go' category but increased among pairs that prefer 'NoGo' category, after passive exposure. Go-Go (orange), pre: 0.067 ± 0.002, post: 0.065 ± 0.002, t = 0.805, df = 24772, p = 0.421; NoGo-NoGo (blue), pre: 0.045 ± 0.004, post: 0.078 ± 0.003, t = 5.345, df = 5329, p < 0.0001. Mean noise correlations increased across neurons that prefer different categories after passive exposure. Go-NoGo (yellow), pre: 0.048 ± 0.002, post: 0.064 ± 0.002. t = 5.924, df = 21743, p < 0.0001. Unpaired t-test for all comparisons.

Comparison of noise correlation matrices before and after learning revealed a similar trend as signal correlation. We found that learning increased noise correlations for pairs of neurons with more similar category preferences (Go-Go, pre: 0.031 ± 0.003, post: 0.141 ± 0.003; NoGo-NoGo, pre: 0.101 ± 0.003, post: 0.153 ± 0.003) (Figures 11E and 11F). On the other hand, cell pairs with opposite preference showed a significant decrease in noise correlations (Go-NoGo, pre: 0.032 ± 0.002, post: -0.006 ± 0.002) (Figures 11E and 11F), consistent with prior observations in primate V1 (Bondy et al., 2018). Passive exposure did not alter noise correlation among Go-Go pairs and slightly

increased noise correlation among Go-NoGo pairs with opposite category preference as opposed to the observed decrease in the active learning group.

Do the learning-induced changes in neuronal correlations persist outside the context of task performance? To address this question, we calculated signal and noise correlation matrices using trials during the out-of-task condition in which animals were satiated, thus not actively performing the task (aka 'Out-of-Task'/OOT; Figures 11A, 11B, 11E, and 11F). Under this condition, 'within-pool' signal and noise correlations (Go-Go and NoGo-NoGo) significantly decreased in magnitude compared with levels during active task performance (Figures 11B and 11F). 'Across-pool' signal and noise correlations (Go-NoGo) also changed during the out-of-task condition to become similar to pre-training levels. Note that the mean noise correlation, which was calculated across all neurons regardless of category preference, slightly increased through active training or passive exposure (Figure 12A) and remained elevated during the out-of-task condition. Therefore, the mean noise correlation alone did not differentiate between active learning versus passive exposure or between task engagement and out-of-task contexts.

Next, we asked whether and how changes in pairwise correlations are related to an animal's behavioral performance. To quantify relative strengths of 'within-pool' versus 'across-pool' correlations in individual animals, we devised a metric called 'correlation block index' (see Methods). Both signal and noise correlation block indices tended to be greater in animals with better behavioral performance (signal correlation, $R^2 = 0.394$; noise correlation, $R^2 = 0.228$), although this observation did not reach statistical significance (Figures 12B and 12C). Taken together, we conclude that

learning increases ‘within-pool’ correlations while decreasing ‘across-pool’ correlations. Critically, this learning-induced re-organization of neuronal correlations is behavioral context-dependent.

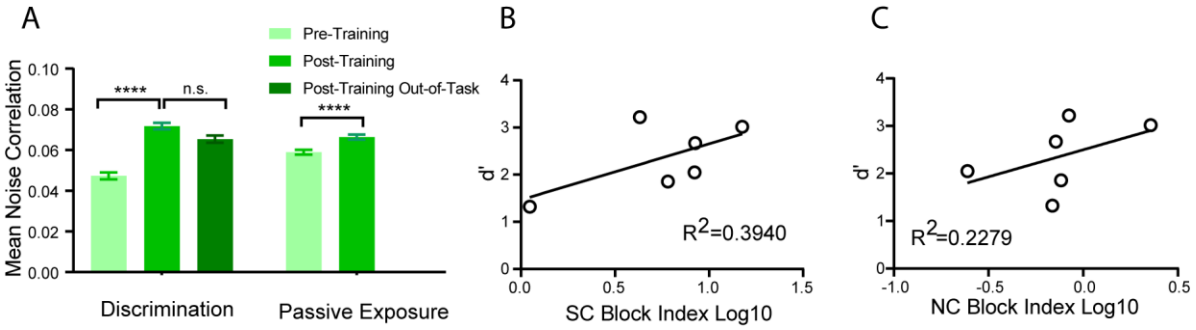

Figure 12. Signal and noise correlation display subtle but positive relation with behavioral performance. (A) Mean noise correlations among all neurons. Discrimination: Pre: 0.047 ± 0.002, n = 18403 pairs, Post: 0.072 ± 0.002, n = 26635 pairs, t = 10.20, p < 0.000001, df = 45036; Post Out-of-Task: 0.065 ± 0.002, n = 15390 pairs, (Post vs. Post Out-of-Task) t = 2.545, p =0.010944, df = 42023, (Pre vs. Post Out-of-Task) t = 7.331, p < 0.000001, df = 33791. Passive Exposure: Pre: 0.059 ± 0.001, n = 22380 pairs; Post: 0.066 ± 0.001, n = 29470 pairs, t = 4.194, p = 0.00027, df = 51848. Unpaired t-tests. (B) Performance of individual mice (d’) plotted against signal correlation block index (see Methods). (R2 = 0.394; p = 0.182) (C) Same as (B) but showing d’ against noise correlation block index (see Methods). (R2 = 0.228; p = 0.338)

2.2.5 Learning Enhances Coupling Between Signal and Noise Correlations in wS1 Neurons

Prior studies suggest that perceptual learning changes the relationship of signal and noise correlations in a direction that reduces noise correlation among highly signal-correlated pairs (Gu et al., 2011; Jeanne et al., 2013). We asked if the observed learning-induced changes in correlation matrices (Figure 11) reflect an altered relationship at the level of individual pairs of neurons. We divided neuronal pairs into subgroups of Go-Go, NoGo-NoGo and Go-NoGo, depending on the preferred category of individual neurons. Consistent with previous studies (Bondy et al., 2018; Cohen and Kohn, 2011; Kwon et al., 2018), there was a significant positive relationship between signal and noise correlations even before training (Figure 13A). Note that signal and noise correlations are not mathematically related, because noise correlation quantifies

trial-by-trial co-fluctuation around the mean evoked response for each stimulus frequency. As Figure 13A-C show, the dots become more widely distributed along noise correlation axis in post-training condition, indicating that noise correlations grew in magnitude through learning among strongly signal-correlated pairs in the ‘within-pool’ subgroups (Go-Go and NoGo-NoGo) (Figures 13A and 13B). On the other hand, strong negative noise correlations emerged among negative signal-correlated pairs in the ‘across-pool’ subgroup (Go-NoGo) (Figure 13C). The clusters of data (i.e. yellow dots) shift from the center to the upper right or lower left corner after learning (Figure 13A-C). The enhanced correlation between neurons of shared category preference could be due to the formation of ‘like-to-like’ local subnetworks among L2/3 neurons, as shown by prior theoretical (Ocker and Doiron, 2019) and experimental works (Khan et al., 2018; Ko et al., 2011; Najafi et al., 2020).

Does the learning-induced reorganization of noise correlations have a functional significance? To address this question, we sub-selected trials based on the animal's behavioral responses and asked if mean noise correlation varied on trials with different responses. Category-specific neurons were defined based on stimulus probability (SP) values (Figure 9A); a neuron whose mean SP ± 95% CI > 0.5 or < 0.5 was respectively defined as a Go or NoGo category-specific neuron (Kwon et al., 2016). Within-pool noise correlations (Go-Go and NoGo-NoGo) increased in magnitude, whereas across-pool noise correlations (Go-NoGo) became more negative on trials in which the animal generated the learned behavioral response (Go-Go: no-lick, 0.230 ± 0.004; lick, 0.300 ± 0.007; NoGo-NoGo: no-lick, 0.221 ± 0.004; lick, 0.242 ± 0.004; Go-NoGo: no-lick, -0.082 ± 0.003; lick, -0.156 ± 0.004 (Figure 13D). One potential explanation is that

learning-induced L2/3 subnetworks of correlated neurons facilitate the conversion of sensory input into learned behavioral responses.

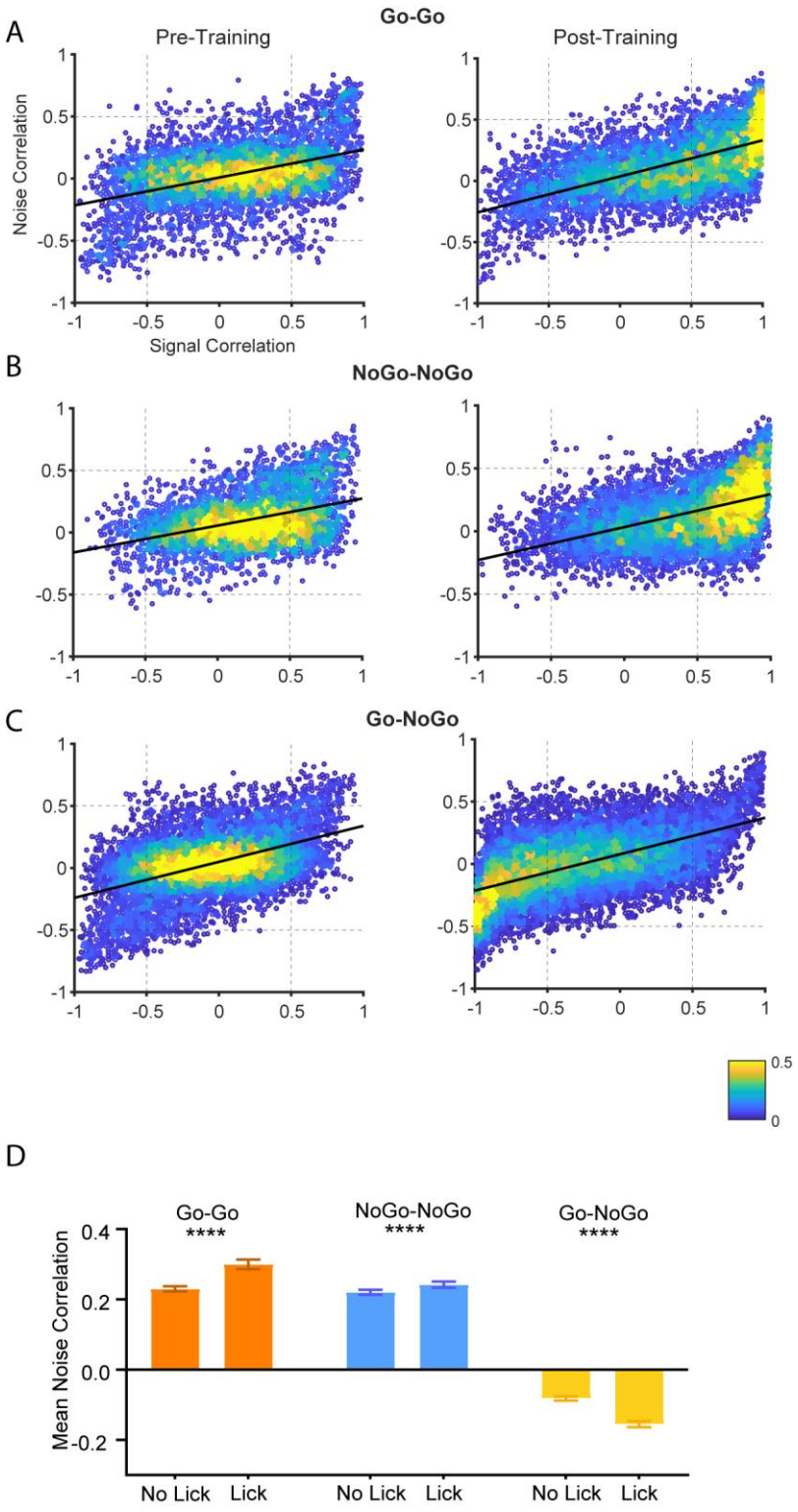

Figure 13. Noise correlations among signal-correlated neurons increase through learning. (A) Heat scatter plot. The color represents the density of data within a 0.04-by-0.04 square. Noise correlation is plotted against signal correlation for neuron pairs that preferentially respond to a Go stimulus frequency. Plots for pre-training (Left, correlation coefficient = 0.421) and post-training (Right, correlation coefficient = 0.594) sessions are shown for comparison. (B) Same as A but for pairs that prefer a Nogo stimulus

*frequency (Pre: correlation coefficient = 0.393; Post: correlation coefficient = 0.475). (C) Same as A but between neurons that prefer different stimulus categories (Pre: correlation coefficient = 0.480; Post: correlation coefficient = 0.576). (D) Mean noise correlation on lick versus no lick trials. ****, p < 0.0001 for all comparisons (paired t test). Go-Go (orange), No-Lick: 0.230 ± 0.004, Lick: 0.300 ± 0.007, t=-11.060, df = 2455, p < 0.0001; NoGo-NoGo (blue), No-Lick: 0.221 ± 0.004, Lick: 0.242 ± 0.004, t=-5.7031, df = 4293, p < 0.0001; Go-NoGo (yellow), No-Lick: -0.082 ± 0.003, Lick: -0.156 ± 0.004, t= 19.181, df = 5630, p < 0.0001 (paired t-test).*

2.2.6 Noise Correlation Impacts Representation of Stimulus Category by wS1 Population Activity

Prior theoretical studies have established that neuronal correlations affect the information content in a population of neurons (Abbott and Dayan, 1999; Panzeri et al., 2022). To understand how learning-induced changes in neuronal correlations impact the population code, we constructed a support vector machine (SVM)-based classifier to decode stimulus categories from L2/3 population activity (Figure 14A). The decoding accuracy was used as a proxy for 'information' represented by the neuronal population. There was not a statistically significant change found in decoding accuracy after passive exposure (p = 0.150; paired *t*-test). On the other hand, learning significantly improved decoding accuracy from 0.652 ± 0.030 to 0.798 ± 0.035 (p = 0.002; paired *t*-test), which closely matched the animal's classification accuracy (mean = 0.836; n = 6) (Figure 14B). To test the impact of noise correlation on population decoding, we selectively removed the noise correlation by shuffling the trial labels separately for each neuron (Figure 14C). Shuffling was nested within each frequency, so the frequency tuning of individual neurons was not altered by this procedure (data not shown). We repeated shuffling for 100 iterations and calculated the decoding accuracy after each iteration. We then asked if the decoding accuracy calculated using pre-shuffled data fell below or went above the mid-95% interval of the 100 post-shuffle accuracy values. In 5 of 6 expert mice trained to perform the discrimination task, shuffling out noise correlation

significantly improved decoding accuracy (Original: 0.820 ± 0.038; Shuffled: 0.884 ± 0.045) (Figure 14E; Table 2). On the other hand, shuffling out the noise correlation did not change or slightly decreased the stimulus decoding accuracy in other task conditions including pre-training and passive exposure (Figure 14E). These results show that the changes in noise correlation associated with learning have a detrimental effect on the encoding of the task-related stimulus category in wS1 population activity, consistent with prior observations (Ni et al., 2018; Valente et al., 2021). Next, we assessed how learning-induced changes in noise correlation impact the decoding of an animal's behavioral choice (to lick or not). To our surprise, shuffling out the noise correlation had mixed effects with no overall change in choice decoding accuracy (Original: 0.827 ± 0.035; Shuffled: 0.827 ± 0.038) (Figure 14F; Table 3). Therefore, learning-induced changes in noise correlation do not impact decoding of an animal's choice from population activity, although they reduce the amount of stimulus information in wS1 L2/3. Together with the results showing that noise correlations are elevated on lick trials (Figure 13D), our results suggest that correlations facilitate the transformation of sensory input into learned behavioral responses despite their detrimental effects on sensory encoding.

Table 2. Accuracy of decoding stimulus category using wS1 population activity before and after discrimination training in the presence or absence of noise correlations. Each row indicates individual mouse. Decoding accuracy for shuffled data was averaged across 100 iterations. The mean accuracy and 95 % confidence interval are shown.

Decoding Accuracy (Stimulus)					
Pre-Training			Post-Training		
Original	Shuffled	95 CI of shuffled	Original	Shuffled	95 CI of shuffled
0.702	0.768	[0.716,0.808]	0.820	0.958	[0.916,0.988]
0.713	0.683	[0.633,0.735]	0.870	0.949	[0.911,0.974]
0.630	0.604	[0.551,0.647]	0.661	0.706	[0.639,0.783]

0.548	0.593	[0.541,0.637]	0.779	0.779	[0.888,0.963]
0.750	0.689	[0.644,0.7330]	0.935	0.975	[0.955,0.990]
0.661	0.681	[0.646,0.716]	0.853	0.784	[0.758,0.811]

Table 3. Accuracy of decoding stimulus category or animal's choice using wS1 population activity in trained animals. Each row indicates individual mouse. Decoding accuracy for shuffled data was averaged across 100 iterations. The mean accuracy and 95% confidence interval are shown.

Decoding Accuracy (Post-Training)					
Stimulus			Choice		
Original	Shuffled	95 CI of shuffled	Original	Shuffled	95 CI of shuffled
0.702	0.768	[0.716,0.808]	0.607	0.671	[0.598,0.740]
0.713	0.683	[0.633,0.735]	0.852	0.839	[0.800,0.878]
0.630	0.604	[0.551,0.647]	0.704	0.689	[0.613,0.758]
0.548	0.593	[0.541,0.637]	0.824	0.911	[0.867,0.949]
0.750	0.689	[0.644,0.7330]	0.955	0.950	[0.920,0.975]
0.661	0.681	[0.646,0.716]	0.800	0.685	[0.633,0.751]

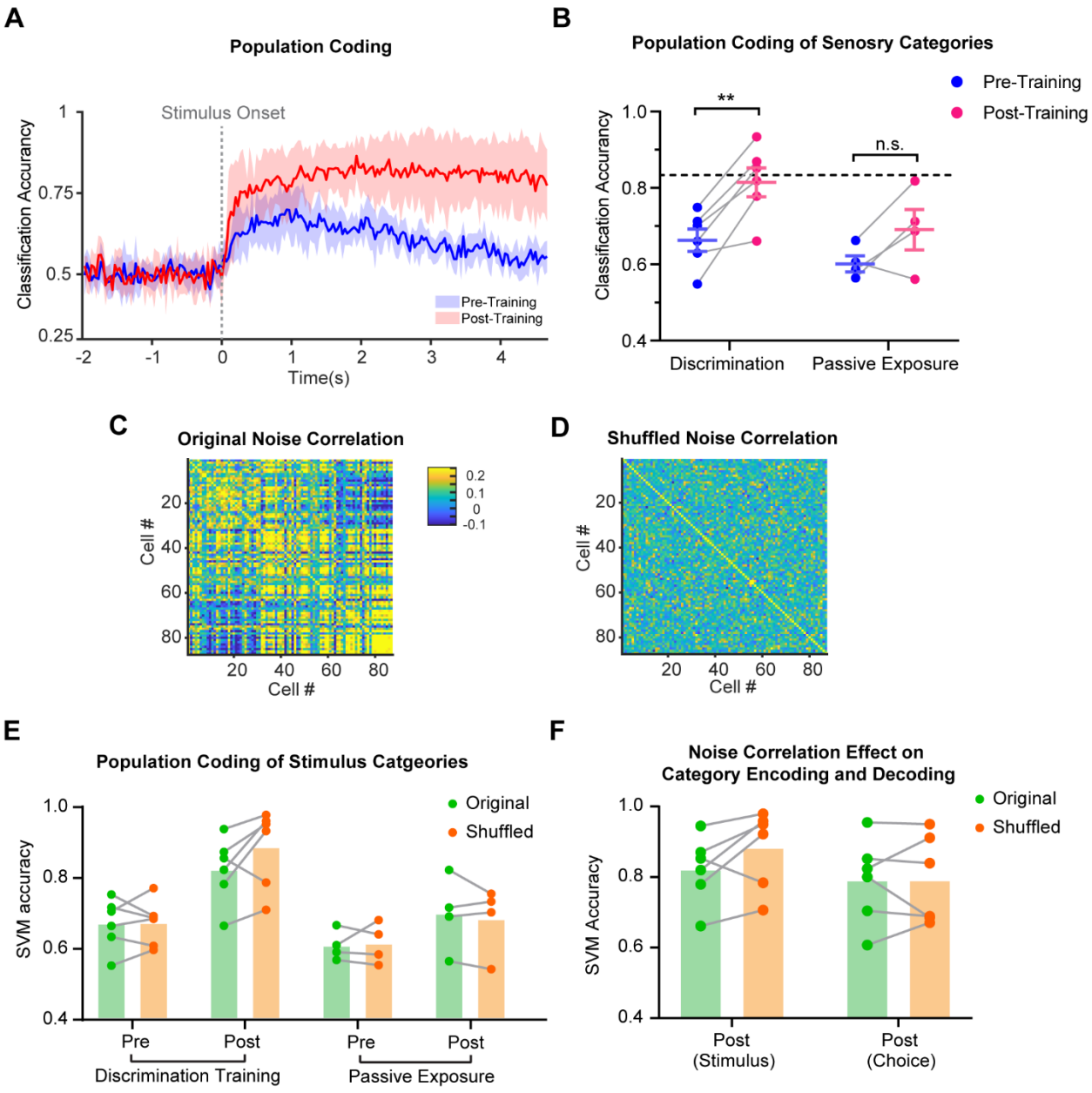

Figure 14. Impact of pairwise correlation on population decoding of stimulus and choice. (A) Performance of a SVM classifier (mean ± SEM across mice) in decoding stimulus category from population activity at each time point of image acquisition. (B) Classification performance reached higher levels in both discrimination learning and passive exposure groups, although the increase was not statistically significant in the passive exposure group. Each dot indicates an animal. Discrimination: pre, 0.667 ± 0.029; post, 0.820 ± 0.021; t = 5.308, df = 5, p = 0.003. Passive exposure: pre, 0.605 ± 0.021; post, 0.695 ± 0.053; t = 1.923, df = 3, p = 0.150. Dashed line indicates expert animal's average performance (0.836, n = 6). Two tailed paired t-tests for all comparisons. (C) Procedure for removing pairwise noise correlation without affecting frequency tuning curves. (top) Example heatmaps showing frequency tuning of individual neurons before and after shuffling trial labels. (bottom) Pairwise noise correlation matrix before and after shuffling trial labels. (D) Performance of a SVM classifier in decoding stimulus category from population activity before and after removing pairwise noise correlation (see Methods). Each dot represents an average Decoding accuracy calculated from 100 iterations normalized to the original Decoding accuracy for each animal. 5 of 6 late-lickers trained to perform the discrimination task showed statistically

significant improvement in Decoding accuracy when noise correlation was removed. On average, decoding accuracy improved from 0.820 ± 0.038 to 0.884 ± 0.045 in post-training group. In all other conditions, the effects were mixed. (E) Comparing impact of removing pairwise noise correlation on decoding stimulus category versus animal's choice from population activity acquired in expert animals (Original: 0.827 ± 0.035; Shuffled: 0.827 ± 0.038; n = 6 mice).

2.2.7 Categorical Neuronal Correlation Structure Also Emerges After Whisker Detection Training

The coding strategy for detecting a range of sensory signal differs slightly from that of discriminating between two similar stimuli. The former may require a higher sensitivity in responding to the signal, while the latter may require a reduction in the overlap of the representations of the two stimuli. It is unclear whether the categorical structure of neuronal correlation is task-specific. To explore the patterns of changes in correlation structures for different sensory processing needs, we trained mice to detect whisker deflection by associating responses to any of nine frequencies with a water reward (Figure 15A). In comparison to the discrimination task, the psychometric curve of the detection task demonstrates a left-shifted detection threshold - between 5Hz and 10Hz (Figure 15B). As mentioned in the approach section, we used two-photon *in vivo* calcium imaging to record neural activity in L2/3 of wS1.

In the detection training paradigm, all nine frequencies are considered GO frequencies, with the exception of 0Hz, which is the only NOGO condition. Interestingly, as shown in Figure 14D, the signal correlation in the whisker detection paradigm demonstrates heterogeneous changes increases among the neurons tuned for low frequencies (i.e. 2 – 20Hz) and among the neurons tuned for high frequencies (i.e. 25 – 50 Hz), and decreases between neuron pairs that are tuned for different ranges of frequencies. The noise correlation also demonstrates a similar structure that the signal correlation has (see Figure 15D). Overall, the range of signal or noise correlations in

post-training detection sessions is smaller than the range in post-training discrimination sessions, which is demonstrated as color shifting in the heatmaps (Figure 15D and 15F). To quantitatively compare the signal and noise correlations after detection training to those after discrimination training, we grouped neurons by their preferred frequencies, with the boundary between 15 Hz and 20 Hz. As shown in Figure 15E-G, detection task training resulted in negative signal and noise correlation 'across' high-low groups, and positive signal and noise correlation 'within' each group. The degree of correlations after detection training was weaker than after discrimination training.

The observation of 'block' formation after whisker detection learning does not completely reject the task-dependency of the changes in neuronal correlation structure. The main reason is that the block observed after whisker detection training shows differences in strength and boundary from the 'blocks' observed after whisker discrimination training. However, it remains unclear why the block forms during detection training and why the boundary is between 20Hz and 25Hz. There are two potential explanations. First, it could be reflecting an intrinsic category defined by mechanoreceptors or thalamic processing, and associative learning allows neurons sharing similar inputs to synchronize with each other. For instance, different behavioral patterns are associated with different whisking rate ranges in mice. During locomotion, mice typically whisk at a rate between 9 and 16 Hz, whereas during intense whisking, the rate can exceed 20 Hz (Jin et al., 2004; Mitchinson et al., 2011; Sofroniew et al., 2014). Second, when all frequencies are rewarded, correlated responses in wS1 reduce the granularity of frequency encoding and facilitate signal propagation.

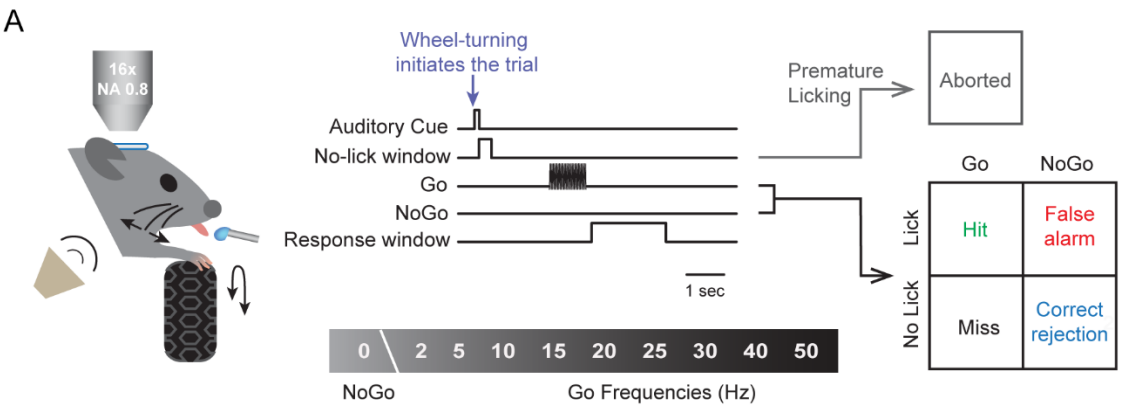
A
16x
NA 0.8
Wheel-turning
initiates the trial
Auditory Cue
No-lick window
Go
NoGo
Response window
1 sec
Premature
Licking
Aborted
Go
NoGo
Lick
No Lick
Hit
False
alarm
Miss
Correct
rejection
0
2
5
10
15
20
25
30
40
50
NoGo
Go Frequencies (Hz)

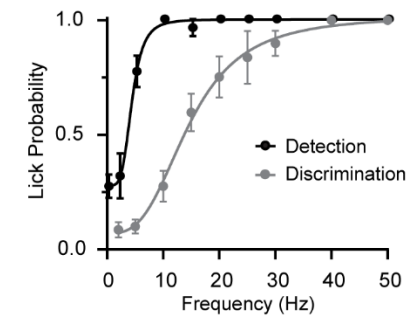
B
Lick Probability
1.0
0.5
0.0
Detection
Discrimination
0
10
20
30
40
50
Frequency (Hz)

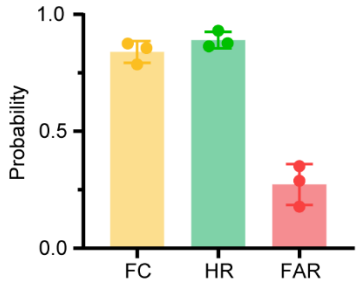
C
Probability
1.0
0.5
0.0
FC
HR
FAR

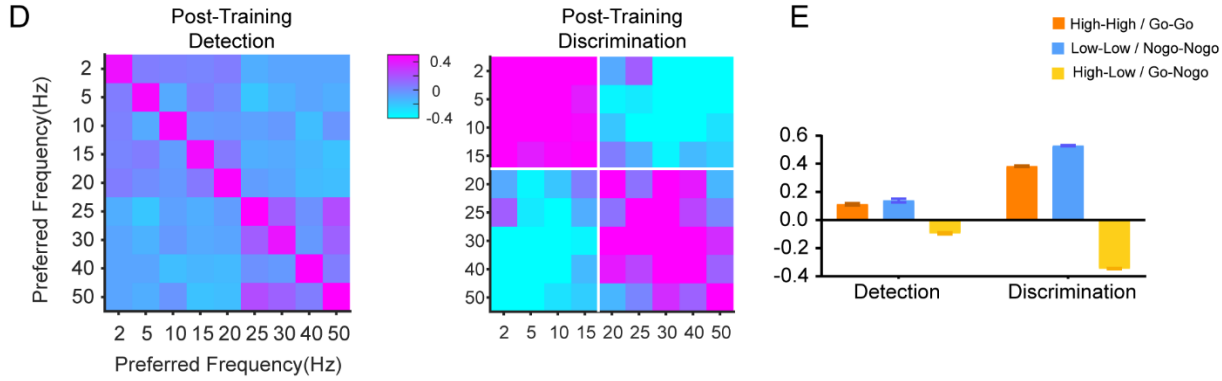
D
Post-Training
Detection
Post-Training
Discrimination
Preferred Frequency(Hz)
2 5 10 15 20 25 30 40 50
0.4
0
-0.4
E
High-High / Go-Go
Low-Low / Nogo-Nogo
High-Low / Go-Nogo
0.6
0.4
0.2
0.0
-0.2
-0.4
Detection
Discrimination

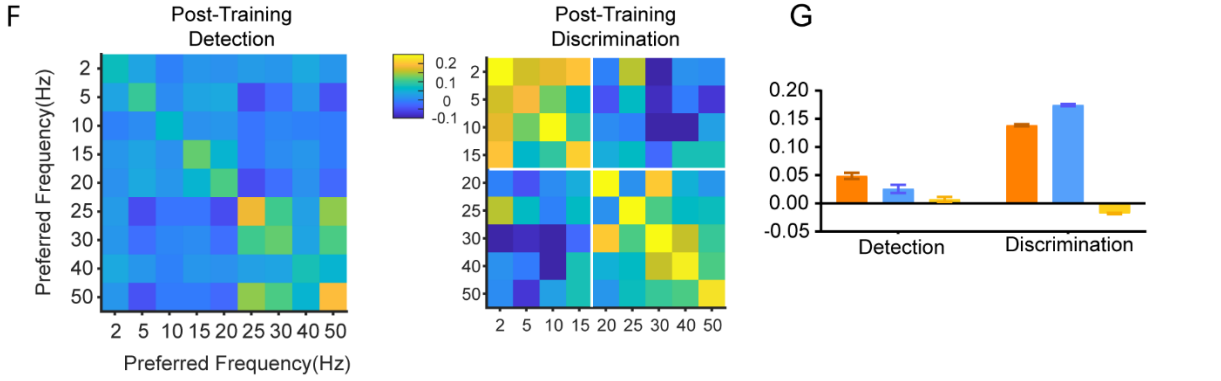
F
Post-Training
Detection
Post-Training
Discrimination
Preferred Frequency(Hz)
2 5 10 15 20 25 30 40 50
0.2
0.1
0
-0.1
G
0.20
0.15
0.10
0.05
0.00
-0.05
Detection
Discrimination

Figure 15. Neuronal correlations also found in wS1 after learning whisker vibration frequency detection task. (A) Same as Figure 6A, except the all nine frequencies are treated as 'GO' and trials without whisker deflection (0Hz) are 'NOGO' trials. (B) Average psychometric function of all animals trained under detection paradigm (black curve, n = 3 mice) and 'High-GO' paradigm (grey curve, n = 6 mice). (C) Average fraction of FC, HR and FAR of expert mice (n = 3 mice). FC: 0.839 ± 0.027; HR: 0.890 ± 0.020; FAR: 0.273 ± 0.051. (D) Color in each bin indicates mean pairwise signal correlation among neurons whose preferred frequency is indicated by x and y coordinate of that bin. Data from post-training detection (left) and discrimination (right) sessions in expert animals. (E) Mean signal correlations in expert animals after training. Detection: High-High (orange), 0.112 ± 0.004; Low-Low (blue), 0.139 ± 0.007; High-Low (yellow), -0.095 ± 0.004. Discrimination: see Figure 10F. (F) Same as panel D but for noise correlation. (G) Mean noise correlations in expert animals after training. Detection: High-High (orange), 0.049 ± 0.003; Low-Low (blue), 0.026 ± 0.004; High-Low (yellow), 0.007± 0.002.

2.3 Discussion

In this study, we demonstrate that training in a wS1-dependent tactile frequency discrimination task results in enhanced representation of task-related (i.e., discriminated) categories in mouse wS1 L2/3 neurons. Neurons gained the ability to represent stimulus categories by broadening their frequency tuning curves. Critically, this learning-induced plasticity was not observed in animals passively experiencing repetitive whisker stimulation, or when actively trained animals were disengaged from the task performance. Task learning increased 'within-pool' neuronal correlations while decreased 'across-pool' correlations such that neurons became increasingly aligned along the direction of stimulus category, indicating increased 'like-to-like' interactions. The learning-induced re-organization of noise correlations had detrimental effects on the amount of sensory information estimated using population decoding accuracy, but it did not constrain an animal's decision during task performance. Furthermore, 'like-to-like' interactions were elevated on trials where trained animals exhibited the decision-related behavior. This indicates that 'like-to-like' interactions may facilitate propagation of sensory information to downstream areas that execute learned behavioral responses, although they simultaneously limit the amount of sensory information within wS1. Taken together, we showed that representation of task-related categories emerges through

changes in selectivity of individual neurons and in the structure of neuronal correlations even at the very first stages of cortical sensory processing. These learning-induced changes likely facilitate propagation of sensory information from primary sensory cortex to downstream areas.

Neurons in the adult mouse primary sensory cortex undergo various forms of plastic changes during learning. Extensive studies in mouse V1 L2/3 have documented an increased selectivity for rewarded stimuli, increased number of responsive neurons, reduced trial-to-trial variability of responses, enhanced encoding of non-sensory task-related variables and various changes in tuning curves (Goltstein et al., 2013; Goltstein et al., 2018; Henschke et al., 2020; Jurjut et al., 2017; Poort et al., 2015). These modifications generally result in enhanced discrimination of target versus foil stimuli and correlate with behavioral performance. Our results extend these findings and demonstrate that wS1 neurons also gain selectivity to task-related categories through learning. A main finding of our study is that cortical plasticity during perceptual learning involves changes in pairwise correlations that become increasingly aligned to task-related categories, indicating formation of task-related neuronal subnetworks in the L2/3 of sensory cortex.

Prior studies suggest that these subnetworks of correlated neurons may play an important role in amplifying relevant stimulus features (Peron et al., 2020), reducing dimensionality of sensory information (Nassar et al., 2021) and enhancing propagation and read-out of sensory information (Valente et al., 2021; Zylberberg et al., 2017). A recent work in mouse posterior parietal cortex demonstrated that correlations can benefit task performance even if they decrease sensory information as they enhance

the conversion of sensory information into behavioral choices (e.g. ref 22). A novel finding of our study is that this functional role of noise correlations is sharpened by learning. This reveals a novel neural mechanism of learning that adds significantly to the previous seminal work on noise correlations and learning (Cohen and Maunsell, 2009; Ni et al., 2018).

The causal role of subnetworks of correlated neurons in early sensory cortex remains to be addressed by manipulating subnetworks in sensory cortex and assessing the impact on downstream areas in the same brain. A recent study has found that an ensemble of neurons in L2/3 of wS1 play a causal role in driving an animal's decision-making during a texture discrimination task (Buetfering et al., 2022). The questions of whether and how L2/3 subnetworks propagate sensory information to downstream areas during decision-making may be tackled using simultaneous optogenetic manipulation and calcium imaging.

Synaptic mechanisms underlying learning-induced category-specific increases in noise correlations remain unclear. A potential source of noise correlations includes local synaptic connectivity (Ko et al., 2014), shared afferent input (Shadlen and Newsome, 1998), feedforward (Kanitscheider et al., 2015) and top-down feedback signals (Bondy et al., 2018). In our study, category-specific increases in signal and noise correlations were only observed during active task performance, which points to top-down feedback as a major source of modulation of correlations. Further studies would be required to dissect contributions of different sources. Neuronal subtypes that participate in the subnetwork of correlated neurons need to be determined. Recent studies suggest that inhibitory INs as well as excitatory neurons participate in cortical subnetworks

(Agetsuma et al., 2018; Khan et al., 2018; Najafi et al., 2020; Wilmes and Clopath, 2019). Excitatory neurons that project to specific downstream areas may be preferentially recruited to the subnetworks (Chen et al., 2015; Kwon et al., 2016; Yamashita and Petersen, 2016). The precise function of different IN and projection neuron subtypes in the formation and maintenance of task-relevant subnetworks needs to be assessed in future studies, using cell type-specific imaging and manipulation methods.

2.4 References

Abbott, L.F., and Dayan, P. (1999). The effect of correlated variability on the accuracy of a population code. Neural Comput *11*, 91-101.

Agetsuma, M., Hamm, J.P., Tao, K., Fujisawa, S., and Yuste, R. (2018). Parvalbumin-Positive Interneurons Regulate Neuronal Ensembles in Visual Cortex. Cereb Cortex *28*, 1831-1845.

Bondy, A.G., Haefner, R.M., and Cumming, B.G. (2018). Feedback determines the structure of correlated variability in primary visual cortex. Nat Neurosci *21*, 598-606.

Buetfering, C., Zhang, Z., Pitsiani, M., Smallridge, J., Boven, E., McElligott, S., and Hausser, M. (2022). Behaviorally relevant decision coding in primary somatosensory cortex neurons. Nat Neurosci *25*, 1225-1236.

Caras, M.L., and Sanes, D.H. (2017). Top-down modulation of sensory cortex gates perceptual learning. Proc Natl Acad Sci U S A *114*, 9972-9977.

Carrillo-Reid, L., Han, S., Yang, W., Akrouh, A., and Yuste, R. (2019). Controlling Visually Guided Behavior by Holographic Recalling of Cortical Ensembles. Cell *178*, 447-457 e445.

Chen, J.L., Margolis, D.J., Stankov, A., Sumanovski, L.T., Schneider, B.L., and Helmchen, F. (2015). Pathway-specific reorganization of projection neurons in somatosensory cortex during learning. Nat Neurosci *18*, 1101-1108.

Cohen, M.R., and Kohn, A. (2011). Measuring and interpreting neuronal correlations. Nat Neurosci *14*, 811-819.

Cohen, M.R., and Maunsell, J.H. (2009). Attention improves performance primarily by reducing interneuronal correlations. Nat Neurosci *12*, 1594-1600.

Corbo, J., McClure, J.P., Jr., Erkat, O.B., and Polack, P.O. (2022). Dynamic Distortion of Orientation Representation after Learning in the Mouse Primary Visual Cortex. J Neurosci *42*, 4311-4325.

Dana, H., Sun, Y., Mohar, B., Hulse, B.K., Kerlin, A.M., Hasseman, J.P., Tsegaye, G., Tsang, A., Wong, A., Patel, R.*, et al.* (2019). High-performance calcium sensors for imaging activity in neuronal populations and microcompartments. Nat Methods *16*, 649-657.

Goltstein, P.M., Coffey, E.B., Roelfsema, P.R., and Pennartz, C.M. (2013). *In vivo* two-photon Ca2+ imaging reveals selective reward effects on stimulus-specific assemblies in mouse visual cortex. J Neurosci *33*, 11540-11555.

Goltstein, P.M., Meijer, G.T., and Pennartz, C.M. (2018). Conditioning sharpens the spatial representation of rewarded stimuli in mouse primary visual cortex. Elife *7*.

Goltstein, P.M., Reinert, S., Bonhoeffer, T., and Hubener, M. (2021). Mouse visual cortex areas represent perceptual and semantic features of learned visual categories. Nat Neurosci *24*, 1441-1451.

Gu, Y., Liu, S., Fetsch, C.R., Yang, Y., Fok, S., Sunkara, A., DeAngelis, G.C., and Angelaki, D.E. (2011). Perceptual learning reduces interneuronal correlations in macaque visual cortex. Neuron *71*, 750-761.

Henschke, J.U., Dylda, E., Katsanevaki, D., Dupuy, N., Currie, S.P., Amvrosiadis, T., Pakan, J.M.P., and Rochefort, N.L. (2020). Reward Association Enhances Stimulus-Specific Representations in Primary Visual Cortex. Curr Biol *30*, 1866-1880 e1865.

Hong, Y.K., Lacefield, C.O., Rodgers, C.C., and Bruno, R.M. (2018). Sensation, movement and learning in the absence of wS1. Nature *561*, 542-546.

Hutson, K.A., and Masterton, R.B. (1986). The sensory contribution of a single vibrissa's cortical barrel. J Neurophysiol *56*, 1196-1223.

Jeanne, J.M., Sharpee, T.O., and Gentner, T.Q. (2013). Associative learning enhances population coding by inverting interneuronal correlation patterns. Neuron *78*, 352-363.

Jin, T E; Witzemann, V and Brecht, M (2004). Fiber types of the intrinsic whisker muscle and whisking behavior. The Journal of Neuroscience 24: 3386-3393

Jurjut, O., Georgieva, P., Busse, L., and Katzner, S. (2017). Learning Enhances Sensory Processing in Mouse V1 before Improving Behavior. J Neurosci *37*, 6460-6474.

Kanitscheider, I., Coen-Cagli, R., and Pouget, A. (2015). Origin of information-limiting noise correlations. Proc Natl Acad Sci U S A *112*, E6973-6982.

Kato, H.K., Gillet, S.N., and Isaacson, J.S. (2015). Flexible Sensory Representations in Auditory Cortex Driven by Behavioral Relevance. Neuron *88*, 1027-1039.

Khan, A.G., Poort, J., Chadwick, A., Blot, A., Sahani, M., Mrsic-Flogel, T.D., and Hofer, S.B. (2018). Distinct learning-induced changes in stimulus selectivity and interactions of GABAergic interneuron classes in visual cortex. Nat Neurosci *21*, 851-859.

Ko, H., Hofer, S.B., Pichler, B., Buchanan, K.A., Sjostrom, P.J., and Mrsic-Flogel, T.D. (2011). Functional specificity of local synaptic connections in neocortical networks. Nature *473*, 87-91.

Ko, H., Mrsic-Flogel, T.D., and Hofer, S.B. (2014). Emergence of feature-specific connectivity in cortical microcircuits in the absence of visual experience. J Neurosci *34*, 9812-9816.

Kwon, S.E., Tsytsarev, V., Erzurumlu, R.S., and O'Connor, D.H. (2018). Organization of orientation-specific whisker deflection responses in L2/3 of mouse somatosensory cortex. Neuroscience *368*, 46-56.

Kwon, S.E., Yang, H., Minamisawa, G., and O'Connor, D.H. (2016). Sensory and decision-related activity propagate in a cortical feedback loop during touch perception. Nat Neurosci *19*, 1243-1249.

Marshel, J.H., Kim, Y.S., Machado, T.A., Quirin, S., Benson, B., Kadmon, J., Raja, C., Chibukhchyan, A., Ramakrishnan, C., Inoue, M.*, et al.* (2019). Cortical layer-specific critical dynamics triggering perception. Science *365*.

Mitchinson, B et al. (2011). Active vibrissal sensing in rodents and marsupials. Philosophical Transactions of the Royal Society of London B: Biological Sciences 366: 3037-3048.

Miyashita, T., and Feldman, D.E. (2013). Behavioral detection of passive whisker stimuli requires somatosensory cortex. Cereb Cortex *23*, 1655-1662.

Najafi, F., Elsayed, G.F., Cao, R., Pnevmatikakis, E., Latham, P.E., Cunningham, J.P., and Churchland, A.K. (2020). Excitatory and Inhibitory Subnetworks Are Equally Selective during Decision-Making and Emerge Simultaneously during Learning. Neuron *105*, 165-179 e168.

Nassar, M.R., Scott, D., and Bhandari, A. (2021). Noise Correlations for Faster and More Robust Learning. J Neurosci *41*, 6740-6752.

Ni, A.M., Ruff, D.A., Alberts, J.J., Symmonds, J., and Cohen, M.R. (2018). Learning and attention reveal a general relationship between population activity and behavior. Science *359*, 463-465.

Ocker, G.K., and Doiron, B. (2019). Training and Spontaneous Reinforcement of Neuronal Assemblies by Spike Timing Plasticity. Cereb Cortex *29*, 937-951.

Panzeri, S., Moroni, M., Safaai, H., and Harvey, C.D. (2022). The structures and functions of correlations in neural population codes. Nat Rev Neurosci *23*, 551-567.

Peron, S., Pancholi, R., Voelcker, B., Wittenbach, J.D., Olafsdottir, H.F., Freeman, J., and Svoboda, K. (2020). Recurrent interactions in local cortical circuits. Nature *579*, 256-259.

Peron, S.P., Freeman, J., Iyer, V., Guo, C., and Svoboda, K. (2015). A Cellular Resolution Map of wS1 Activity during Tactile Behavior. Neuron *86*, 783-799.

Poort, J., Khan, A.G., Pachitariu, M., Nemri, A., Orsolic, I., Krupic, J., Bauza, M., Sahani, M., Keller, G.B., Mrsic-Flogel, T.D.*, et al.* (2015). Learning Enhances Sensory and Multiple Non-sensory Representations in Primary Visual Cortex. Neuron *86*, 1478-1490.

Sachidhanandam, S., Sreenivasan, V., Kyriakatos, A., Kremer, Y., and Petersen, C.C. (2013). Membrane potential correlates of sensory perception in mouse wS1. Nat Neurosci *16*, 1671-1677.

Schoups, A., Vogels, R., Qian, N., and Orban, G. (2001). Practising orientation identification improves orientation coding in V1 neurons. Nature *412*, 549-553.

Schumacher, J.W., McCann, M.K., Maximov, K.J., and Fitzpatrick, D. (2022). Selective enhancement of neural coding in V1 underlies fine-discrimination learning in tree shrew. Curr Biol *32*, 3245-3260 e3245.

Shadlen, M.N., and Newsome, W.T. (1998). The variable discharge of cortical neurons: implications for connectivity, computation, and information coding. J Neurosci *18*, 3870-3896.

Stringer, C., and Pachitariu, M. (2019). Computational processing of neural recordings from calcium imaging data. Curr Opin Neurobiol *55*, 22-31.

Sofroniew, N J; Cohen, J D; Lee, A K and Svoboda, K (2014). Natural whisker-guided behavior by head-fixed mice in tactile virtual reality. The Journal of Neuroscience 34: 9537-9550.

Valente, M., Pica, G., Bondanelli, G., Moroni, M., Runyan, C.A., Morcos, A.S., Harvey, C.D., and Panzeri, S. (2021). Correlations enhance the behavioral readout of neural population activity in association cortex. Nat Neurosci *24*, 975-986.

Wilmes, K.A., and Clopath, C. (2019). Inhibitory microcircuits for top-down plasticity of sensory representations. Nat Commun *10*, 5055.

Xin, Y., Zhong, L., Zhang, Y., Zhou, T., Pan, J., and Xu, N.L. (2019). Sensory-to-Category Transformation via Dynamic Reorganization of Ensemble Structures in Mouse Auditory Cortex. Neuron *103*, 909-921 e906.

Yamashita, T., and Petersen, C. (2016). Target-specific membrane potential dynamics of neocortical projection neurons during goal-directed behavior. Elife *5*.

Yang, H., Kwon, S.E., Severson, K.S., and O'Connor, D.H. (2016). Origins of choice-related activity in mouse somatosensory cortex. Nat Neurosci *19*, 127-134.

Zylberberg, J., Pouget, A., Latham, P.E., and Shea-Brown, E. (2017). Robust information propagation through noisy neural circuits. PLoS Comput Biol *13*, e1005497.

Chapter 3 Discussion, Significance, and Outlooks

My dissertation study developed a novel tactile discrimination Go/Nogo behavioral task that enables detailed psychometric and neuromeric analyses over a wide range of task-related frequencies. An important feature of this task is the 'self-initiation' at the beginning of each trial, which ensures animals' engagement in the task when stimuli were delivered. A major strength of my study is the comparison of neural activity and neuron-neuron interaction across four different behavioral contexts: (1) passive exposure of repeated stimuli, (2) expert animals performing the discrimination task, (3) expert animals satiated and no longer licking but passively receiving stimuli, and (4) expert animals performing the detection task that uses the same set of stimuli as the discrimination task.

One caveat of the experiment design is that it doesn't exclude the possibility that higher frequencies intrinsically trigger stronger responses in mice. Ideally, we can change the reward contingency to lower frequencies as an alternative experimental group. In the preliminary study, the low-'GO' group experienced significantly longer training time which results an uncontrollable observing window. Although challenging to train, two-alternative forced choice behavioral paradigm treats two behavioral categories distinctively but equivalently, making it a suitable protocol for studying learning effect of sensory neural representations. It is also worth mentioning that previous findings reported that rodent encodes both the amplitude and frequency of whisker deflection. In

my study, the amplitude of deflection has been kept the same while the frequency varies. A reasonable critic could be that varying frequencies with constant amplitude aren't equivalent. Future study could explore different combinations of stimulating duration, amplitude, and frequency to achieve equivalence stimuli.

Another puzzle of this study is the quick recovery of performance 4 days post contralateral wS1 ablation. There could be multiple routes for the animal to recover sensory discrimination a few days after the surgical ablation of contralateral wS1. For example, the animal could generalize the learned sensory task to both hemispheres of the brain. One way of testing it is to deliver the selected frequency to whiskers on the other side of the face and see if the categorical behavioral outcome remains.

The main results of my study indicate that perceptual learning induces plasticity in both the stimulus selectivity of the neurons and the structure of signal and noise correlations such that signal-correlated neurons – i.e. neurons with similar frequency tuning – increase noise correlations (trial-to-trial co-fluctuation). Our analysis shows that, while enhanced noise correlations among similarly tuned neurons limit the amount of sensory information encoded in the sensory cortex, they have little impact on the animal's decision. Taken together, learning-induced enhancement of neuronal correlations in the sensory cortex will facilitate task performance potentially through robust propagation of the task-relevant signals to downstream brain areas despite a reduced capacity of sensory representation.

The potential mechanism of the emergence of task-relevant correlations remains unclear. On one hand, category-specific increases in signal and noise correlations were induced by learning and only observed during active task performance, which points to

top-down feedback (e.g. motor planning, reward related feedback, etc.) as a driver of task-related subnetworks. On the other hand, the fact that some task-related neuronal correlations remained enhanced during OOT sessions suggests that there are alternative sources driving plasticity. Differential changes of signal and noise correlations after detection training indicate the possibility of intrinsic connectivity as an alternative driver to shape the plasticity in L2/3 of wS1. To further understand the source and function of neuronal coding, it would be important to investigate cell type-specific correlations and relate the structure of neuron-neuron correlation to synaptic connections in wS1. Additionally, recording what activity is transmitted to downstream brain regions given the learning-induced correlational structure is another key issue to tackle.

In summary, my research establishes useful behavioral paradigms and presents novel findings that advance our understanding of sensory coding by neuron population. In a larger context, the advancement of understanding neuronal codes can lead to circuit-level biomarkers that can potentially benefit diagnosis and treatment of complex neurological disorders.